July 31, 2016 Docket: PROJ0769

U.S. Nuclear Regulatory Commission
ATTN: Document Control Desk
One White Flint North
11555 Rockville Pike
Rockville, MD 20852-2738

SUBJECT: NuScale Power, LLC Submittal of Topical Report TR-0516-49417, "Evaluation Methodology for Stability Analysis of the NuScale Power Module," Revision 0 (NRC Project No. 0769)

REFERENCES: Letter from NuScale Power, LLC to U.S. Nuclear Regulatory Commission, "Final Schedule for Topical Report Submittals," LO-0616-50035, dated June 30, 2016 (ML16182A532).

In Reference 1, NuScale Power, LLC (NuScale) provided an updated schedule for topical report submittals. NuScale provided a schedule indicating the intent to submit this topical report by July 31, 2016. Consistent with that schedule, NuScale hereby submits Topical Report TR-0516-49417, "Evaluation Methodology for Stability Analysis of the NuScale Power Module," Revision 0.

The purpose of this submittal is to request NRC review and approval of the methodology presented in this report as an acceptable method to demonstrate primary system stability of the NuScale Power Module. NuScale respectfully requests that the acceptance review be completed in 60 days from the date of transmittal.

Enclosure 1 contains the proprietary version of the report entitled "Evaluation Methodology for Stability Analysis of the NuScale Power Module." NuScale requests that the proprietary version be withheld from public disclosure in accordance with the requirements of 10 CFR § 2.390. The enclosed affidavit (Enclosure 3) supports this request. Enclosure 1 has also been determined to contain Export Controlled Information. This information must be protected from disclosure per the requirements of 10 CFR Part 810.

Enclosure 2 is the nonproprietary version of the report entitled "Evaluation Methodology for Stability Analysis of the NuScale Power Module."

This letter makes no regulatory commitments and no revisions to any existing regulatory commitments.

Please feel free to contact Jennie Wike at 541-360-0539 or at jwike@nuscalepower.com if you have any questions.

Sincerely,

Thomas A. Bergman
Vice President, Regulatory Affairs
NuScale Power, LLC

Distribution:

Frank Akstulewicz, NRC, TWFN-6C20
Greg Cranston, NRC, TWFN-6E7
Omid Tabatabai, NRC, TWFN-6E7
Mark Tonacci, NRC, TWFN-6E7

Enclosure 1: “Evaluation Methodology for Stability Analysis of the NuScale Power Module”, TR-0516-49417-P, Revision 0, proprietary version
Enclosure 2: “Evaluation Methodology for Stability Analysis of the NuScale Power Module”, TR-0516-49417-NP, Revision 0, nonproprietary version
Enclosure 3: Affidavit, AF-0716-50372

Enclosure 1:

"Evaluation Methodology for Stability Analysis of the NuScale Power Module," TR-0516-49417-P, Revision 0, proprietary version

NuScale Power, LLC
1100 NE Circle Blvd., Suite 200 Corvallis, Oregon 97330 Office 541.360-0500 Fax 541.207.3928
www.nuscalepower.com

Enclosure 2:

"Evaluation Methodology for Stability Analysis of the NuScale Power Module," TR-0516-49417-NP, Revision 0, nonproprietary version

NuScale Power, LLC
1100 NE Circle Blvd., Suite 200 Corvallis, Oregon 97330 Office 541.360-0500 Fax 541.207.3928
www.nuscalepower.com

Licensing Topical Report

Evaluation Methodology for Stability Analysis of the NuScale Power Module

July 2016

Revision 0

Docket: PROJ0769

NuScale Power, LLC

1100 NE Circle Blvd., Suite 200

Corvallis, Oregon 97330

www.nuscalepower.com

© Copyright 2016 by NuScale Power, LLC

Licensing Topical Report

COPYRIGHT NOTICE

Licensing Topical Report

Department of Energy Acknowledgement and Disclaimer

This material is based upon work supported by the Department of Energy under Award Number DE-NE0000633.

CONTENTS

TABLES

FIGURES

Abstract

This NuScale Power, LLC, (NuScale) topical report presents a methodology to address thermal-hydraulic stability in the NuScale Power Module (NPM) as a basis to demonstrate compliance with the applicable regulations. This report considers stability phenomena from the fundamental level and describes computational methods for the analysis of the postulated instability modes of the NPM during steady-state normal operation and anticipated transients.

NuScale requests approval of the computational methods described in this topical report for demonstrating the stability performance of the NPM and approval of the regional exclusion approach based on maintaining subcooling in the riser for protecting the onset of instabilities in the NPM. This topical report is not intended to provide final design values or evaluation of stability. Rather, example values for the various evaluations are provided for illustrative purposes in order to aid the reader's understanding of the context of the application of this methodology.

Executive Summary

This NuScale topical report presents a methodology for addressing thermal-hydraulic stability in the NPM as a basis to demonstrate compliance with 10 CFR 50 General Design Criteria (GDC) 10, GDC 12, and Design Specific Review Standard Section 15.9.A “Thermal Hydraulic Stability Review” (Reference 12.1.2) for thermal-hydraulic stability. The basis of the NPM stability study is a detailed phenomenological review, which identifies the following:

- possible modes of instability and the limiting instability mode
- operating conditions that may result in instability
- generic representations of anticipated transients where unstable oscillations may occur

The phenomenological review identifies the limiting instability mode as natural circulation instability. For the limiting instability mode, the adiabatic riser response dominates the response rather than wave propagation in the core. The dynamics of the steam generator (SG) and the fission power response to reactivity feedback influence stability. This report emphasizes the important distinctions from the familiar density wave instabilities in boiling water reactors (BWRs). Specifically, the report emphasizes that the reactivity feedback is stabilizing in the NPM, and that the increase in core inlet subcooling is not destabilizing, as is the case in BWR instability.

This report presents a description of the computational method for the analysis of the postulated instability modes of the NPM during steady-state normal operation and anticipated transients. The technical approach selected for the stability protection solution in the NPM that is demonstrated in this report is the regional-exclusion type, not the detect-and-suppress type. The operational domain identified with potential instability is characterized by loss of subcooling in the riser that leads to vapor generation in the chimney above the core, which is excluded by the module protection system (MPS) protective actions.

This fundamental level computational method is the basis for the PIM code. The objective of the PIM code is to simulate the dynamics of the flow in the NPM coolant loop with attention to optimal resolution of its stability. Predictions of the PIM code are compared with the NuScale Integral System Test (NIST-1) facility test results to demonstrate the capability of the code to predict accurate stability results. Stability tests were conducted at the NIST-1 facility to assess primary system stability performance. A comparison of the NIST-1 test data is provided to demonstrate that the PIM code predictions have a conservative bias for the predicted decay ratio of primary system flow peaks that occur immediately after a feedwater flow perturbation. This report provides a discussion of how this approach demonstrates acceptability of the PIM code as a conservative predictive model for stability analysis of the NPM. Additionally, the report describes how the stability tests performed in the NIST-1 facility demonstrate the stable response of the scaled test facility for primary system stability.

The demonstrative examples in the report identify that no instabilities occur over the range of power evaluated as long as a loss of riser subcooling does not occur. The methodology credits MPS actuation to preclude onset of instability on loss of subcooling with sufficient margin to accommodate instrumentation lags and other effects that delay the occurrence of a reactor trip.

This topical report provides an acceptable methodology for performing the following:

- disposition of potential modes of instability in the NPM that affect the primary system
- acceptable computational methods to demonstrate the stability of the NPM for modes not already dispositioned in the context of addressing GDC 12. Specifically, the computational methods are acceptable for showing the reactor core and associated coolant, control, and protection systems ensure that power and hydraulic oscillations that can result in conditions exceeding specified acceptable fuel design limits are not possible. This includes:
    - the methodology is acceptable for demonstrating that the NPM is stable in the region identified with single phase flow in the riser
    - the methodology of stability protection by regional exclusion is acceptable. The MPS enforces the regional exclusion by using safety-related systems for ensuring the NPM maintains adequate riser subcooling relative to the saturation temperature at the pressurizer pressure. The MPS automatic action is actuated by the loss of core exit subcooling (high temperature or low system pressure), which is relied on to protect plant operations for events other than stability

The methodology described in this report utilizes design features and parameters as assumptions. NuScale is not requesting approval for these features or parameters as part of the review of this report.

1.0 Introduction

1.1 Purpose

The purpose of this report is to present an evaluation methodology for the stability analysis of the NuScale Power Module (NPM), assess the analysis tools versus stability test data, and introduce the stability protection solution that ensures occurrence of instability is precluded in the NPM. This report forms the analysis methodology for addressing stability considerations in the primary system of the NPM.

1.2 Scope

This report starts with a concise description the NPM to provide a frame of reference for the stability issues related to its operation. The scope of the stability evaluation covers a general review of instability modes and phenomena to narrow down and focus the concepts with regard to their applicability to the NPM. Thereafter, a physical and mathematical model for simulating the NPM dynamic response, with special attention to the resolution of the oscillation phenomena, is described from first principles and the numerical embodiment in a computer code is presented. Next, example numerical results are provided that demonstrate the inherent stability of the NPM utilizing the methodology described in this report. These results are provided as an example of the basic elements of a stability protection solution that complies with the applicable regulations.

In summary, the scope of this report covers the following topics:

- a general description of the design features that are utilized in the stability methodology
- a review of stability phenomena that apply to the NPM
- a physical, mathematical, and numerical description of the models implemented with the PIM code that is used in performing calculations of NPM stability performance
- a summary of test data from the NIST-1 facility and comparisons of the analysis tool results versus the NIST-1 test data
- example results from demonstrative calculations of the NPM stability performance
- a conclusion based on the above results supporting a stability analysis methodology

The example analyses performed in this topical report utilize the current NPM design and performance, including data for the following:

- geometric design

- operating conditions
- nuclear kinetics parameters and reactivity coefficients for beginning and end of an equilibrium fuel cycle
- MPS settings and delays
- event sequences
- critical heat flux modeling

As described above, the PIM code is used in performing calculations of NPM stability performance. The PIM code is maintained in accordance with the NuScale quality assurance program (Reference 12.1.1). Underlying elements of the quality assurance program describe the software configuration control and software change processes.

1.3 Abbreviations

Table 1-1. Abbreviations

Term	Definition
AOO	anticipated operational occurrence
BOC	beginning of cycle
BWR	boiling water reactor
CHF	critical heat flux
CVCS	chemical and volume control system
EOC	end of cycle
GDC	General Design Criteria
MPS	module protection system
MTC	moderator temperature coefficient
NIST-1	NuScale Integral System Test
NPM	NuScale Power Module
NRC	Nuclear Regulatory Commission
NSSS	nuclear steam supply system
PWR	pressurized water reactor
RCS	reactor coolant system
RPV	reactor pressure vessel
SAFDL	specified acceptable fuel design limit
SG	steam generator

Table 1-2. Definitions

Term	Definition
Decay ratio	The measure of the change of peak amplitude of an oscillation relative to that of the previous oscillation. A stable system has a decay ratio less than unity, meaning oscillations resulting from a perturbation decay with time.
Moderator reactivity coefficient	The coefficient of reactivity related to change in moderator conditions. Typically expressed in terms of moderator temperature for a single-phase system, it can equivalently refer to changes in moderator density. A negative moderator reactivity coefficient implies that reactivity decreases with increasing moderator temperature or decreasing moderator density.

2.0 Background

The dynamic behavior of a nuclear power plant is a critical design and licensing consideration. Operational and design basis considerations require that any nuclear plant behaves in a reliable way when mildly disturbed (i.e., a disturbance in which the plant is not automatically shut down by control rod motion). Feedback mechanisms should ensure that the plant responds by transitioning to a new state upon being disturbed, where stable operations are established at the new operating state. If this stable operation after disturbance cannot be ensured, then protective measures are necessary to ensure safety of the plant.

Boling Water Reactors (BWRs) are known to exhibit unstable operation in certain circumstances that require rapid response of plant protection systems to prevent fuel damage. This response can either come in the form of a reactor trip if the plant enters an exclusion region or by detecting the onset of instabilities through plant instrumentation and then suppressing the oscillations by a reactor trip. Forced circulation Pressurized Water Reactors (PWRs) do not exhibit this behavior. However, the NPM is a PWR designed to operate using natural circulation as the means of providing core coolant flow. This use of natural circulation motivates added consideration for the potential of unstable operation, which is addressed with the stability analysis methodology.

This topical report describes the stability analysis methodology in the context of addressing specific regulatory requirements. Specifically, this report describes a computational method that is designed to address stability-related issues and uses generally accepted numerical approaches and phenomenological models. In addition to the physical modeling, the code has many special features that enable a stability calculation to quickly attain a converged steady-state configuration from a wide range of different conditions. The attained steady state does not have to be physically correct (e.g., at the initiation of two-phase flow condition), but such cases are performed to explore effects such as two-phase flow and SG performance on stability. Of particular importance, the code can attain a converged steady-state configuration even if the system is in an unstable condition. Various different perturbation mechanisms can then be applied to the converged system that test the stability performance and assist in identifying cause and effect.

2.1 Regulatory Requirements

The methodology is applied to demonstrate compliance with Title 10 of the Code of Federal Regulations Part 50 (10 CFR 50), Appendix A "General Design Criteria for Nuclear Power Plants," Criteria 10 and 12.

Design Specific Review Standard 15.9.A, "Thermal Hydraulic Stability Review," (Reference 12.1.2) for hydraulic stability provides the detailed guidance. The guidance for stability with respect to the NPM is to:

- evaluate potential power and hydraulic stability mechanisms
- disposition those mechanisms for which extensive evidence exists that operation is not affected
- describe a methodology for demonstrating acceptable performance relative to GDC 12 and specified acceptable fuel design limits (SAFDLs)

3.0 General Plant Description

The following sections provide a brief description of a single NPM as a background for the rest of the report addressing the neutronic and thermal-hydraulic stability. Design aspects not related to stability are not included in the description.

3.1 NuScale Power Module

The NPM is a self-contained nuclear steam supply system (NSSS) comprised of a reactor core, a pressurizer, and two SGs integrated within the reactor pressure vessel (RPV) and housed in a compact steel containment vessel (CNV). The NPM is designed to operate at full-power conditions using natural circulation as the means of providing core coolant flow, eliminating the need for primary coolant pumps. The reactor core is located inside a core barrel connected to the hot leg riser. The reactor core heats primary coolant causing the coolant to flow upward through the riser. When the heated primary coolant exits the riser, it passes over the tubes of the helical coil SGs, which act as a heat sink. As the primary coolant passes over the SG tubes, it cools, increases in density, and naturally circulates down to the reactor core, where the cycle begins again.

The NPMs are partially immersed in a reactor pool that serves as the ultimate heat sink. Each NPM has a dedicated chemical and volume control system (CVCS), emergency core cooling system, and decay heat removal system.

Important features of the NPM include the following:

- An integral PWR NSSS that combines the reactor core, SGs, and pressurizer within the RPV. Unlike a conventional PWR, this design eliminates the external piping necessary to connect the SGs and pressurizer to the RPV.
- Buoyancy forces that drive natural circulation of the primary coolant, eliminating the need for primary coolant pumps.

3.2 Nuclear Steam Supply System

The NSSS consists of the reactor core, helical coil SGs, and a pressurizer within a single pressure vessel. The NSSS is enclosed in a cylindrical CNV that sits in the reactor pool structure. The reactor core is located below the helical coil SGs inside the RPV. Using natural circulation, the primary coolant flow path is upward through the riser, and then downward around the SG tubes followed by return to the bottom of the core via an annular downcomer. As the primary coolant flows across the outside of the SG tubes, heat is transferred to the secondary side fluid inside of the SG tubes. The secondary side fluid is heated, boiled, and superheated to produce steam for the turbine generator unit.

3.3 Reactor Pressure Vessel

The RPV consists of a steel cylinder with an inside diameter of approximately 9 ft and is designed for an operating pressure of approximately 1850 psia. To provide a barrier between the saturated water in the pressurizer and the primary coolant system fluid, a steel pressurizer baffle plate is integral with the SG tube sheets and the RPV. The pressurizer baffle plate is integrated with the upper steam plenum, has orifices to allow in and out surges of water, and to act as a thermal barrier.

3.3.1 Steam Generator

The NPM uses two once-through helical-coil SG units for steam production. The SG is located in the annular space between the hot leg riser and the RPV inside diameter wall. The SG tubes are connected to feed and steam plena with tube sheets. Preheated feedwater enters the lower feed plenum through nozzles on the RPV. As feedwater rises through the interior of the SG tubes, primary coolant adds heat, and the feedwater experiences a phase change and exits the SG as superheated steam (Figure 3-1).

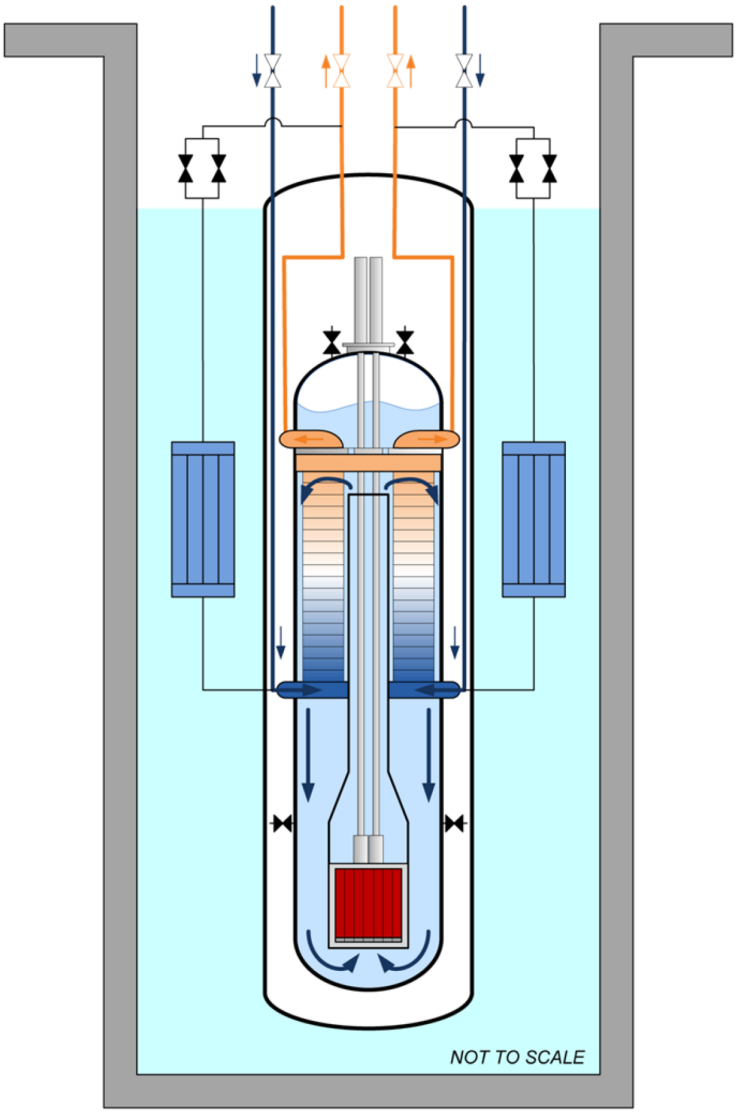

Figure 3-1. Steam Generator and Reactor Flow

3.3.2 Pressurizer

The pressurizer provides the means for controlling primary system pressure. The design of the pressurizer is to maintain a constant primary coolant pressure during operation. Applying power to a bank of heaters installed above the pressurizer baffle plate increases primary system pressure. Pressure in the primary coolant system is reduced using spray provided by the CVCS.

3.3.3 Reactor Core

The core configuration for the NPM consists of 37 fuel assemblies, 16 of which include control rod assemblies. The fuel assembly is a standard 17x17 PWR fuel assembly with 24 guide tube locations for control rod fingers and a central instrument tube. The assembly is nominally half the height of standard plant fuel and several spacer grids provide support. The fuel is UO_2 with Gd_2O_3 as a burnable absorber homogeneously mixed within the fuel for select rod locations. The U^{235} enrichment is below 4.95 percent.

3.4 Chemical and Volume Control System

The CVCS is not required to function during or after an accident. During normal operation, the CVCS recirculates a portion of the primary coolant through demineralizers and filters to maintain primary coolant cleanliness and chemistry. A portion of the recirculated coolant supplies pressurizer spray for controlling reactor pressure. Injection of additional water controls primary system coolant inventory when primary coolant levels are low, during letdown of primary coolant to the liquid radioactive waste system, or when coolant inventory is high. Additionally, during the module start-up process, the CVCS adds heat to the primary coolant via the module heatup heat exchanger (also referred to as the startup heater) to establish natural circulation flow in the primary coolant system.

3.5 Startup and Shutdown

Figure 3-2 illustrates an example of the module startup path on a pressure-temperature plane. During startup, the operating domain pressure and temperature are increasing under CVCS heating and conditions are confined to a {{

}}$^{2(a),(c)}$

{{

}}2(a),(c),ECI

Figure 3-2. Example Pressure-Temperature Operating Domain

3.6 Primary and Secondary Operating Conditions

Primary and secondary steady-state operating conditions are determined by engineering evaluations for a wide range of operating power levels. The evaluations address a number of design considerations, including control strategy (constant core inlet, average, or outlet temperature as a function of power) and SG operating conditions considering the desired steam temperature. Predictions are made for the NPM best-estimate primary coolant flow rates as functions of reactor power level. As described in Section 10.0, the application methodology addresses revisions to the best-estimate primary flow rate and addresses the effects of design minimum and maximum flow rate.

The steady-state operating conditions incorporate the effects of ambient heat losses and heat loss through non-regenerative heat exchange in the CVCS. {{

}}2(a),(c),ECI The heat loss in the CVCS non-regenerative heat exchanger is

assumed to be {{ }}$^{2(a),(c)}$ These heat losses are not critical, except as they reduce the total heat transferred to the secondary system.

Representative primary initial conditions at rated power are as follows:

{{

}}$^{2(a),(c)}$

Table 3-1. Primary Steady-State Conditions

{{

}}2(a),(c),ECI

Representative secondary system steady conditions at off-rated power are chosen consistent with expected plant operations, including transition of secondary conditions at {{

}}2(a),(c),ECI

These conditions consider the effects of heat losses described earlier.

3.7 Module Protection System

The NPM is equipped with a safety-related MPS that contains a full complement of subsystems to evaluate safety-related process measurements for compliance with specified limits. The MPS initiates protective measures when specified limits are exceeded. In establishing limits to be used in the analytical demonstration of the MPS performance, consideration for instrumentation response times, instrument uncertainty, calibration intervals, and other effects is made to ensure the required safety measures, such as safety limits for SAFDLs, are protected over a wide range of anticipated operational occurrences (AOOs) and accidents.

The safety logic for performing a reactor trip is the primary protective measure for stability-based events in the NPM. The main safety-related process measurements for the reactor trip that play a role in protecting stability-based events are as follows:

- ex-core measurement of neutron flux
- hot leg temperature as measured at the top of the riser section
- pressurizer pressure
- pressurizer level
- primary system flow

Other process measurements for SG secondary and containment conditions are also present, but are not expected to play a role in protecting stability-related events.

The MPS compares the above process measurements to specified limits to determine if a trip should occur using the following signals:

- high power
- high count rate
- high startup rate
- high power rate
- high hot leg temperature
- high pressurizer pressure
- high pressurizer level
- low pressurizer pressure
- low pressurizer level

- low low primary system flow

Any of the above signals that exceed their specified limits are expected to result in a reactor trip.

Setpoints used in the analytical demonstration of the MPS performance for protecting the plant consider effects of uncertainties and delay times. Demonstrating these analytical setpoints is a main function of nuclear safety analysis activities and depends on a wide range of design input, including physical sensor design and placement, electrical system design, time for breakers to open couplings to release the control rods, and time for the control rods to physically enter the core.

Typical sensor response times used in determining analytical limits are {{

}}$^{2(a),(c)}$

Table 3-2. Assumed Safety Sensor Response Times

{{

}}$^{2(a),(c)}$

While other MPS actuations may occur earlier than the times cited in Table 3-2, the demonstration analysis described in this report utilizes the hot leg temperature instrument combined with sensed pressure to provide an MPS trip that actuates when {{ }}$^{2(a),(c),ECI}$

The analyses use a total reactor trip delay time of 10 seconds from the time of physically exceeding the setpoint to start of control rod insertion. As described in Section 10.0, the application methodology addresses MPS settings and delays found in plant technical specifications and other sources.

4.0 Phenomenological Description of NuScale Power Module Stability

4.1 Introduction

As described in Section 3.0, the NPM is an integral PWR. The SG is integrated within the RPV and the primary coolant flow is driven by natural circulation, which is an important aspect of its passive design philosophy. The density difference between the relatively high temperature flow exiting the core and the lower temperature flow returning through the downcomer annulus where the SG is the heat sink creates the natural circulation driving head. This configuration presents {{

}}$^{2(a),(c),ECI}$

Various feedback mechanisms are included, and special consideration is given to the possible coupling of the SG dynamics and the flow stability in the primary loop. Feedback coupling between the thermal-hydraulic phenomena and the neutron kinetics is important where coolant and fuel rod temperatures provide reactivity feedback, and the core power response affects the coolant temperature and the density head that drives the flow and influences its stability. Pure neutronic stability, without thermal-hydraulic feedback coupling, is addressed separately in dedicated neutronic analyses in the design certification.

4.2 Background and Past Reactor Stability Studies

Open literature contains extensive studies of the stability of nuclear systems, which is only a subset of the larger body of work when industrial activities in this area by reactor and fuel vendors are included. The primary focus of historical stability work has been for

BWRs, where complex interactions of coolant density waves and nuclear reactivity may lead to flow and power oscillations – a condition that must be excluded for normal operation and licensing of the reactor.

Reference 12.1.3 by Lahey and Drew provides an early survey of the literature on stability analysis and experimental data related to light water reactors. This extensive review covers a wide range of data and analytical methods and instability types in two-phase flow. The classification of physical instability mechanisms in Reference 12.1.3 is an expanded version of the one given in the review article by Bouré *et al.* (Reference 12.1.4). Lahey and Drew enlarged Bouré *et al.* classification by including nonlinear phenomena where supercritical Hopf bifurcation leads to finite amplitude limit cycle oscillations and subcritical bifurcation leads to the possibility of divergent oscillations if the initial perturbation is sufficiently large even when the initial state is linearly stable. Professor Hennig and his associates cover the topic of nonlinear oscillations for BWR conditions in several works (e.g., Reference 12.1.5). Lahey and Drew also included neutron reactivity coupled thermal-hydraulic instabilities, for which a later, more detailed monograph on the specific instability mode of nuclear-coupled density waves is given in Reference 12.1.6. A comprehensive review of BWR stability given in Reference 12.1.7 is another example of the stability work in the nuclear industry. The works cited are examples from a large body of literature that focuses on boiling flows, and does not mention single-phase flow instabilities. Nevertheless, the review provides a useful reference on the methodology of instability mode classification and a guide on how to approach stability analysis problems in the NPM design, in which natural circulation under single-phase flow conditions is the normal operation mode and substantial voiding is outside the range of intended operation.

The flow stability in PWRs has also been addressed in literature. A recent example in Reference 12.1.8 for a large forced-circulation PWR, identified and summarily dispositioned certain instability modes. Tong and Weisman (Reference 12.1.9) covered the topic of stability as part of their monograph book on PWR thermal analysis. As part of their stability discussion, they provided a classification of possible instabilities. A comprehensive review of natural circulation flow phenomena, including stability, of light water cooled nuclear plants sponsored by the IAEA with contributions from many leading experts in the field is found in Reference 12.1.10. Stability of natural circulation flow of two-phase and single-phase systems is covered with regards to phenomena, models, and experiments in test loops. Of the most interest are Annex 7 through 10. The IAEA report also provides tabulated classification of instability modes. Instability classification can be also found in the recent review article by Prasad *et al.* (Reference 12.1.11).

The methodology presented in this report is based on {{

}}[2(a),(c)] Once the potential instability modes are identified, the phenomena governing the various feedback mechanisms are recognized for inclusion in the governing equations of mathematical and numerical models.

Section 4.3 presents a typical instability classification and provides notes on the relevance of each mode for the NPM and the method for disposition or further in-depth analysis.

4.3 Instability Mode Classification

The instability modes are broadly classified as static or dynamic. Each category lists the instability modes and provides a description of the mechanism for each mode. The instability mode's relevance to the NPM is evaluated and determined as not applicable, excluded as limited by other phenomena, or applicable. For instability modes identified as applicable, a disposition or detailed analysis is presented, as appropriate.

4.3.1 Static Instabilities

There are no instabilities that are strictly static; rather, the definition of a static instability requires that inertia effects are not important. Static instabilities refer to transitions among operating states that are all valid solutions of the steady-state balance equations of a flow system. Dynamic models are inherently able to detect static instability modes even though the momentum conservation that is part of the dynamic models does not play an important role. Examples of static instabilities include flow excursion (Ledinegg instability), flow regime relaxation instability, and geysering.

4.3.1.1 Instability Mode: Flow Excursion (Ledinegg)

Description: In its original description, flow excursion (Ledinegg) instability is a type of static instability that is determined by the relationship between the pressure drop characteristic of a boiling channel and the pressure drop characteristic imposed by an external system (e.g., a pump). An operating point is unstable if

$$\left.\frac{d\Delta P}{d\dot{m}}\right|_{internal} \leq \left.\frac{d\Delta P}{d\dot{m}}\right|_{external} \qquad \text{Eq. 4-1}$$

where

$\dot{m}$ = mass flow rate
ΔP = pressure drop

The subscript *internal* refers to the sum of pressure drop components along the flow path and the subscript *external* refers to the external drive or a pump.

The condition given in Eq. 4-1 is possible only if the pressure drop as function of mass flow rate is not a monotonic function and Ledinegg instabilities are caused by the particular S-shape that the pressure drop versus flow rate characteristic that may be exhibited by a boiling channel.

{{

}}2(a),(c),ECI

Evaluation: This mode is applicable in principle and a disposition is given below.

There is no possibility for negative slope of the $\Delta P(\dot{m})$ curve in the case of single-phase natural circulation and it can be demonstrated that in a substantially unconstricted flow path like the primary circuit in the NPM that this condition is also absent even under two-phase conditions. Figure 4-1 plots the flow characteristic function $\Delta P(\dot{m})$ for several power levels in which the pressure drop components are calculated for best-estimate models of the NPM using PIM. {{

}}2(a),(c),ECI It is demonstrated that there is no negative slope at any power at the steady-state balanced loop operating points where $\Delta P = 0$. Moreover, negative slope is not found on the curve. Therefore, the flow excursion mode is not possible in the NPM.

Conclusion: Since there is no possibility for negative slope of the $\Delta P(\dot{m})$ curve in the case of single-phase natural circulation, the flow excursion mode cannot cause instabilities within the NPM. No further consideration of this instability mode is required within the stability analysis methodology.

{{

}}2(a),(c)

Figure 4-1. Pressure Residual as Function of Total Flow Rate at Different Power Levels

4.3.1.2 Instability Mode: Boiling Crisis

Description: Boiling crisis occurs when a power increase results in a higher heat flux than the flux that can be transferred by nucleate boiling. The state of the coolant in contact with the fuel rod surface undergoes oscillations between the nucleate and film boiling regimes.

Evaluation: This thermal instability is mentioned in this report for completeness only. The main reason for avoiding instabilities is to avoid reaching the point where boiling crisis may occur and fuel damage may occur. Reactor operation is restricted such that a margin to boiling transition is achieved by maintaining the minimum critical heat flux (CHF) ratio above correlation limits.

Conclusion: Since the CHF ratio is maintained above correlation limits, the boiling crisis mode cannot cause instabilities in the NPM. No further consideration of this instability mode is required within the stability analysis methodology.

4.3.1.3 Instability Mode: Flow Pattern Transition (Relaxation) Instability

Description: Flow regime transitions could in principle influence the pressure drop and create inflections of the pressure drop versus flow rate that might result in instability under certain conditions. Flow regime transitions include laminar-to-turbulent transitions and bubbly-to-annular flow transitions.

Evaluation: {{

}}$^{2(a),(c)}$Bubbly-to-annular flow regime transitions occur at high steam qualities and are outside the operational range of the NPM, which is single-phase flow with minimal, if any, local subcooled boiling. As shown later, other instability modes become excited at lower steam quality in the NPM riser and, therefore, the boiling regime transitions are bounded by these other phenomena.

Conclusion: The effects of flow regime transition are incorporated in the Ledinegg instability evaluation in Section 4.3.1.1 and that mode cannot cause instabilities within the NPM. Therefore, no further consideration of this instability mode is required within the stability analysis methodology.

4.3.1.4 Instability Mode: Flashing Instability

Description: For heaters located under a tall, adiabatic riser where the hot liquid entering the riser experiences a gradual decrease in static pressure as it travels up the riser, the reduction in pressure results in evaporation (flashing), which increases the driving head. The flow increase lowers the temperature of the liquid entering the riser and the flashing is suppressed, which reduces the driving head and lowers the flow to the effect that heater exit temperature increases and the cycle is repeated.

Evaluation: This instability mode is observed only in low-pressure systems with pressures lower than NPM operating pressure, but may be encountered during the startup of a natural circulation BWR. Therefore, this mode is not applicable to the NPM as a primary instability mechanism.

Conclusion: Although not applicable as a primary instability mechanism in the NPM due to the high operating pressure of the primary system, {{

}}$^{2(a),(c)}$

4.3.1.5 Instability Mode: Geysering

Description: The description of the mechanism for geysering in the literature varies, in which the common features are periodic, or chaotic, oscillations due to cyclical vapor generation in a tall riser. The main difference between geysering and flashing instabilities is that in geysering the vapor is generated first in the heater section. Part of the geysering mechanism is the thermodynamic metastable liquid states in which liquid can become superheated (liquid temperature higher than saturation) due to low flow and lack of nucleation sites, and the equilibration occurs suddenly, generating large volumes of

vapor. In addition, the generation of a vapor slug may be attributed to subcooled boiling in the heater section.

Evaluation: Geysering instability is possible only in low-pressure systems with pressures lower than NPM operating pressure, and therefore, is not an applicable primary instability mode in NPM.

Conclusion: Although not an applicable primary instability mechanism in the NPM due to the high operating pressure of the primary system, {{

}}[2(a),(c)]

4.3.2 Dynamic Instabilities

The NPM is a dynamical system that can be modeled using a set of state variables. These state variables include the parameters that define the flow field, such as liquid and vapor mass flow rates and temperatures, core thermal power, and heat flux. Depending on the model order, these variables can be defined at a number of locations in the NPM. The dynamical system is defined by a set of ordinary differential equations where the time derivative of each state variable is given as a generally nonlinear function of the state variable and any constraints, such as boundary conditions and external controls. The functions that determine the time derivatives of the state variables are obtained from the laws governing the physical phenomena, such as the applicable conservation laws and the equations governing fission reaction rates. In the case of a steady state corresponding to given external control, the time derivatives of the state variables vanish and the resulting system of equations can be solved for the set of the state variables (a point in the phase space). A point in the phase space corresponding to steady state is a fixed point. {{

}}[2(a),(c)]

The stability of a dynamical system refers to its behavior in the neighborhood of fixed points. A perturbation of one or more of the state variables at a fixed point introduces nonzero time derivatives and initiates a transient response. The system is stable if the system returns to the fixed point, either monotonically or while undergoing oscillations of decreasing magnitude. Linear stability is defined by the system returning to its fixed point following a small perturbation. Conversely, a linearly unstable system diverges exponentially from its initial fixed point either monotonically or by undergoing oscillations about the fixed point with exponentially growing amplitude. Monotonic divergence is not possible as it can occur only due to positive feedback mechanisms that are excluded by design; for example reactivity coefficients must be negative. Even in certain operating conditions where the boron concentration is high and moderator temperature reactivity coefficient is positive, the overall reactivity coefficient is negative when accounting for Doppler reactivity. Conversely, negative feedback mechanisms may lead to oscillatory behavior that can diverge if the feedback is delayed and sufficiently strong. A diverging

oscillation is the type that is possible in principle and has to be prevented for normal operation.

Nonlinear stability analysis refers to the system behavior in response to a large perturbation that can be induced externally or that results from the growth of a small perturbation of a linearly unstable fixed point. Nonlinear effects can limit the divergence of an oscillation (supercritical Hopf bifurcation, Reference 12.1.5) and the system settles into a stable limit cycle oscillation. It is also possible in principle for a subcritical Hopf bifurcation, that the nonlinear effects accelerate the growth of oscillation magnitude as the oscillation magnitude grows (Reference 12.1.12). For the latter case, a stable fixed point can become unstable given an initial perturbation of sufficiently large magnitude.

{{

}}2(a),(c),ECI

{{

}}2(a),(c)

In the following sections, specific dynamic instabilities are discussed and evaluated according to their respective relevance to the NPM. These sections also provide the phenomenological background for understanding the prevalent instability modes and defining the requirements for the nonlinear time-domain tool to embody the NPM dynamical system.

4.3.2.1 Instability Mode: Pressure Drop Oscillations

Description: Pressure drop oscillations are the dynamic extension of Ledinegg static instability. For both instabilities, pressure drop versus flow rate is a multi-valued function. In the Ledinegg case, a flow excursion occurs once, bringing the flow from an unstable operating point to one or another stable point, depending on the direction of the perturbation. In the pressure drop oscillation, the transition from one flow state to the other is accompanied by a storage mechanism, such as compressing a volume of vapor, which causes a delayed rebound and cyclical transitions ensue.

Evaluation: The necessary condition of a multi-valued pressure drop versus flow rate has been evaluated for the NPM as part of the Ledinegg analysis and found to be unconditionally stable.

Conclusion: The effects of pressure drop oscillations are incorporated in the Ledinegg instability evaluation in Section 4.3.1.1 and that mode cannot cause instabilities within the NPM. Therefore, no further consideration of this instability mode is required within the stability analysis methodology.

4.3.2.2 Instability Mode: Acoustic Oscillations

Description: The mechanism for propagating the disturbances responsible for the acoustic oscillation instability is pressure waves in contrast to density waves, which are discussed separately where the disturbance travels with the flow. Standing pressure waves (sound waves) are resonant where the frequency is determined by the sound speed and the length of the pipe that acts as an organ pipe. The frequency is usually high due to the high speed of sound waves which is sensitive to vapor content. The energy that feeds and sustains the instability is thermal in nature. In the compression phase, direct contact between the liquid phase and the heated surface is forced by collapsing a vapor film and heat transfer is enhanced, while in the rarefaction phase, the vapor film is reestablished, and the cycle is repeated. High velocity flow may also provide the mechanical energy to excite the standing waves.

Evaluation: There is no mechanism for feeding and sustaining this type of instability in the NPM {{

}}$^{2(a),(c),ECI}$ No high velocity flow is present in the NPM circulation loop.

Conclusion: No further consideration of acoustic instability is required in the stability analysis methodology since the mode cannot be sustained in the NPM.

4.3.2.3 Instability Mode: Density Waves

Description: Density wave instability is the most studied of instability mechanisms due to its relevance to BWRs. The instability may occur in vertical heated channels with or without boiling. The fundamental mechanism of the instability is that any flow perturbation at the inlet generates effects that propagate (wave) up the channel. A perturbation decreasing the inlet mass flow rate results in increasing the flow enthalpy,

which also lowers the density either by liquid expansion in the case of single-phase flow or through increased vapor generation. At steady state or quasi-steady state, or for low frequency perturbation, the inlet flow perturbation generates a negative feedback so that the system returns to its initial state and is stable. Specifically, a perturbation decreasing the inlet mass flow rate results in lowering the density in the channel, thus increasing the buoyancy pressure head, which tends to restore the original flow rate. However, the situation is different depending on the frequency of the perturbation in which delayed feedback, if sufficiently strong, can be destabilizing. The delay mechanism is the time it takes for the propagating density wave to transverse the heated channel length. There is a resonant frequency at which the delayed effects of the perturbation reach the channel exit at the time when the inlet perturbation reverses phase, and the original perturbation is reinforced. At this frequency, the system is destabilized, given sufficiently strong feedback, which can occur when the power is increased. For a single-phase heated channel, instability is conceivable only for long heated channels as the density change of liquid due to change in enthalpy is relatively small. Conversely, boiling increases the mixture density response to enthalpy change, making a boiling channel less stable compared to the single-phase case. In addition, in the two-phase case, the feedback from an initial inlet flow perturbation is not limited to density head, but includes the response of friction pressure drop, which is significant due to the two-phase multiplier.

The stability of density waves in a vertical boiling channel depends on the geometry and operating conditions of the system. Specifically, increasing power and decreasing flow are destabilizing. Axial power shapes skewed towards the inlet are also destabilizing. High pressure suppresses the density difference between the liquid and vapor phases and is therefore stabilizing. Increased inlet flow resistance is stabilizing, while increased exit resistance is destabilizing. The distinction is attributed to the phase difference of their respective effects due to the propagating wave. Inlet subcooling has a mixed effect; for highly subcooled flow, further increase of subcooling is stabilizing as it suppresses boiling in a larger part of the channel, but for low subcooling the system is destabilized by increasing inlet subcooling. {{

}}[2(a),(c)] By contrast, single-phase systems are insensitive to inlet subcooling and insensitive to pressure, as long as pressure does not drop to the point where vapor generation (flashing) may occur.

Evaluation: Density wave instability is seldom observed without compounding factors in nuclear systems. In a BWR, the phenomena are complicated by the nuclear reactivity feedback mechanisms and the time delay inherent in the heat conduction of fuel elements. While density waves are present normally in a heated channel, they can occur in a heated channel connected to a tall adiabatic riser as in simplified BWR's with natural circulation. Theoretically, the latter case is not particularly special if the adiabatic riser is

simply considered as part of a single channel with varying geometry where the heating axial distribution is pushed down. Another compounding effect is flashing. Flashing may occur in a tall riser located atop a heated section because the reduced static head lowers the pressure below the saturation point corresponding to the liquid enthalpy at the heated section exit, and induces vapor generation as the liquid travels up the riser. By analogy, flashing has the same effect on stability as a heat source generating vapor, making the riser effectively no longer adiabatic in this aspect.

Conclusion: Density wave phenomena are important for assessing the stability of both the primary coolant flow and the secondary side of the SG of the NPM. Density wave instability is a concern for the flow in the secondary side of the SG of the NPM and must be addressed. Density waves in the primary circuit are part of a compound interconnected phenomena of a potential natural circulation riser instability and must be addressed as an integral process with various components in the stability analysis methodology.

4.3.2.4 Instability Mode: Xenon Oscillations

Description: Xenon oscillation instability is a pure neutronic phenomenon. The products of U^{235} fission include isotopes that are high neutron absorbers or decay into other isotopes that are high neutron absorbers. In this way, fission product poisoning creates a delayed feedback system. A fission product of particular interest is iodine (I^{135}), which is radioactive and decays into Xe^{135}. The latter is a neutron poison with a large neutron absorption cross-section. Thus, decay of I^{135} generates Xe^{135} that is removed by either decaying or absorbing a neutron.

The neutron absorption reaction that removes Xe^{135} constitutes a positive feedback process in which increased fission power leads to increased reactivity, which reinforces the original power increase perturbation. However, the power increase perturbation also generates I^{135}, which decays into Xe^{135} and introduces negative reactivity, a delayed negative feedback process.

Detailed analysis of the xenon reactivity indicates the possibility of unstable power oscillations with a large period. These oscillations may involve the total reactor power or a spatial mode of the power distribution. These spatial modes are the radial (first azimuthal neutron flux mode) and the axial modes. For large PWR cores, the most susceptible mode is the axial oscillations in which the power swings from the top to the bottom of the core. In some PWRs with large cores, direct control to dampen axial xenon oscillations is accomplished using axial shaping control rods. Small cores are more stable in comparison.

Evaluation: Xenon stability calculations for the NPM core demonstrate that these oscillations are highly stable as a pure instability mode. {{

}}$^{2(a),(c),ECI}$ Thus, interaction between the xenon oscillation and thermal-hydraulic feedback is precluded.

Conclusion: Xenon oscillations are unconditionally stable in the NPM core and no further consideration is required in connection with compounding other possible instability modes within the stability analysis methodology.

4.3.2.5 Instability Mode: Natural Circulation Instability

Description: Flow instability in a natural circulation loop bears some resemblance to that of density waves. While the density wave refers to the flow in a heated channel with fixed or prescribed boundary conditions, the natural circulation system includes two legs: a riser and a downcomer. The dynamics of the flow in the two legs depends on the heater design and the heat sink (exchanger) and their respective location. The natural circulation instability mechanism described in this report is for a natural circulation loop in which the heater is located under a tall riser and the cooling heat exchanger is located near the top of the cold leg. In steady state, the temperature in the riser is uniform and higher than the temperature downstream of the heat exchanger, and the corresponding difference in their respective densities create the force driving the flow. The steady-state temperature difference is proportional to the power-to-flow ratio and the friction pressure drop around the loop is proportional to the square of the flow rate; therefore, the steady-state natural circulation flow is proportional to the cubic root of the power. A perturbation increasing the flow rate results in a reduction in the heater exit temperature and an increase in its density. The density perturbation travels up the riser and there is a time delay before the new density is distributed throughout the entire length of the riser. This delayed feedback is negative because the difference in temperature between the riser and the cold leg is diminished and consequently reduces the density difference that drives the flow. If this delayed negative feedback is sufficiently strong, the flow is destabilized and undergoes growing oscillations. In the case of high friction in the loop that reduces flow, or if power input is sufficiently increased, boiling in the riser can be induced. The density response to an enthalpy perturbation is higher in the case of phase change than the case of single-phase thermal expansion by nearly a factor of six for water at the NPM operating pressure. The boiling natural circulation loop can be destabilized more readily than a single-phase loop.

The most idealized natural circulation loop in the literature is the Welander problem (References 12.1.10, 12.1.13, and 12.1.14). The Welander loop is symmetric with the heater located at the bottom of the loop and the heat sink at the top of the loop, thus there is no preference for the direction of the steady-state flow. The flow can be destabilized and oscillate with increasing magnitude and when flow reversal occurs, the flow transitions to oscillating around a negative flow rate point; these transitions were found to exhibit chaotic behavior. The Welander problem is a one-dimensional version of the older Bénard problem of a horizontal layer of fluid heated from below (Reference 12.1.15). While the Welander problem is a simple one, the numerical results were reported to vary and deviate from the experimental observations due to truncation errors and application of diffusive algorithms.

Evaluation: Reference 12.1.16 provides a more detailed analytical evaluation of the natural circulation loop with simplifying assumptions.

Conclusion: Natural circulation instability is a possible mode for the NPM and needs to be evaluated in depth in the stability analysis methodology. The evaluation in this report addresses this mode as well as other compounding phenomena. These compounding phenomena include the feedback from nuclear reactivity and the dynamics of the heat exchanger. Detailed numerical algorithms and models are used to avoid artificial damping, which overestimates the stability of the physical system.

4.3.2.6 Instability Mode: Thermal Stratification Oscillations

Description: For purposes of the NPM, thermal stratification oscillations are a specific extension of natural circulation instability that may occur in an ill-designed system, such as when the heat source is located in a higher elevation than the cooling sink. In such a configuration, heating of the water does not induce a reliable buoyancy-induced flow. Instead, the liquid becomes stratified and a periodic back-and-forth oscillatory flow occurs.

Evaluation: The necessary condition of having the heat source positioned higher than the cooling source does not occur in the NPM. The nuclear core is located sufficiently low in the system that SG heat removal and ambient heat losses out of the vessel do not result in thermal stratification oscillations. {{

}}$^{2(a),(c),ECI}$

Conclusion: No further consideration of this instability mode is required within the stability analysis methodology since the necessary conditions to cause this mode to occur do not exist in the NPM.

4.3.3 Coupled (Compound) Instability Modes

Fundamental, or pure, instability modes that have been presented above can manifest themselves in systems with the geometry and physical properties that permit the mechanisms for the respective mode to operate without interference of other phenomena. By contrast, the compound instability modes include secondary phenomena that influence or modify the primary mechanism significantly. The secondary phenomena may be geometric in nature, or physical processes that interact with the primary mechanisms through feedback that may reinforce or weaken the primary instability or modify its nature. The stability of engineering devices are more likely to require the study of compound instability phenomena, unlike laboratory experiments, which are often performed on simplified apparatuses to resolve the fundamental mechanisms.

4.3.3.1 Instability Mode: Parallel Channel Instability

Description: When a fundamental instability mechanism is possible in a single heated channel (e.g., density waves), the situation is complicated by having several such channels connected to common plena. The common plena alter the boundary conditions under which a single channel would have operated. The common pressure drop boundary condition allows for multiple oscillation modes depending on the phase

difference among the oscillations in each channel. For example, if the flow in all channels oscillates in phase, the stability of the group of channels would be the same as a single channel. However, for two channels oscillating out of phase, the common pressure drop fluctuation is eliminated (in the linear limit) as the effects of the flow oscillations in the two channels cancel out. The fixed pressure drop boundary condition is destabilizing and therefore a set of two channels connected in parallel are less stable than a single one. In the case of three channels, the preferred phase difference is 120 degrees to maintain constant pressure drop between the plena (Reference 12.1.6). For four tubes, two preferred mode possibilities exist: either the channels oscillate with a phase difference of 90 degrees from one to the next, or two groups of two channels each oscillate out of phase while the channels in each group oscillate in phase with one another. The parallel channel instability mode is not necessarily tied to density waves. The compound effect is purely geometrical if the channels are identical, but a richer spectrum of phenomena can be expected in the more general case in which the channels differ in geometry or the power level and distribution.

Evaluation: {{

}}$^{2(a),(c),ECI}$ It was shown in Reference 12.1.17 that this type of instability is dispositioned for PWR conditions using the simplified conservative model of Ishii (Reference 12.1.18). The neutron reactivity feedback is not needed for analyzing this mode as the destabilization leading to flow oscillations in a single channel does not significantly excite a reactor power response.

Conclusion: Parallel channel instability in the {{

}}$^{2(a),(c),ECI}$

The parallel channel instability in the NPM core has been shown not to be a concern and further consideration is not required in the stability analysis methodology.

4.3.3.2 Instability Mode: Primary Circuit Flow Coupling to Secondary Side Steam Generator

Description: {{

}}2(a),(c),ECI

Evaluation: This primary-secondary coupling is of interest if the unstable oscillations in the SG tubes are in phase, which is not the case because the tubes are coupled together through common plena. This forces out-of-phase oscillations that cancel out the net heat sink oscillations. Appendix A addresses additional aspects of this compound phenomenon.

SG secondary side flow coupling to the primary system-side flow is restricted to the effects of the total secondary flow. Out-of-phase flow oscillations in the tubes are self-cancelling and result in no net oscillatory effects. A change of the secondary flow by a forcing function boundary condition influences the primary coolant flow, but the reverse is not possible.

Conclusion: The feedback loop between the SG and the primary side is broken in the NPM. Therefore, no further consideration of possible destabilizing effects of primary-secondary resonances is required in the stability analysis methodology. However, the effects of an externally driven oscillation in the SG are addressed to show their influence on the primary system. Section 8.2.7 addresses the effects of oscillating feedwater flow.

4.3.3.3 Instability Mode: Neutronic Coupling to Natural Circulation Instability

Description: Natural circulation instability was described earlier only considering thermal-hydraulic phenomena. This mechanism is evaluated as a compound instability by taking the effects of the neutron reactivity feedback into account. In response to a flow increase perturbation at the core inlet, the core exit temperature is reduced if the core power is kept constant. The reduction of the average coolant (moderator) temperature introduces positive reactivity and the power is increased for the condition of a negative moderator reactivity feedback. The power increase offsets the core exit temperature reduction and the reactivity response becomes milder (reduced gain). However, the time delay involved in these processes could result in reinforcing the perturbation if the resulting phase shift is large. The case of BWR neutronic coupling destabilizes density waves because the fluctuation in the energy added to the coolant through heat flux at the surface of the fuel rods is delayed relative to the originating fluctuation in the fission heat generation due to the radial heat conduction in the fuel rods. This time delay is {{

}}2(a),(c),ECI

{{

}}2(a),(c),ECI

Conclusion: The reactivity-to-power and power-to-heat flux phenomena are important for the NPM stability performance and are included in the stability analysis methodology.

4.3.3.4 Instability Mode: NuScale Natural Circulation Instability

Description: The components of this compound instability were presented earlier. Specifically, the stability of the flow in a natural circulation loop is first considered with simplifying assumptions of constant heater power and constant density cold leg (due to an idealized perfect heat exchanger/SG). The added phenomena include the reactivity-to-power feedback. Further, the ideal SG assumption is relaxed where realistic modeling of the heat transfer dynamics is considered. {{

}}2(a),(c),ECI The system may include parts in which the flow is two-phase due to subcooled boiling in the core and flashing in the riser, depending on the operating conditions under investigation. The combination of the core with neutronic power feedback, an adiabatic riser where density waves propagate with possible flashing, and {{
}}2(a),(c),ECI constitute a dynamical system that is best modeled numerically.

Evaluation: The main instability mode is the NPM natural circulation instability, also called riser instability mode. The evaluations rely on detailed numerical techniques where a dynamical system is constructed using the:

- nonlinear differential equations governing the conservation of mass, momentum, and energy of the generally two-phase flow field
- equations governing the fission power dynamics
- equations governing heat transfer

Section 5.0 describes the model. Sections 8.0 and 9.0 present results for various representative operating conditions and sensitivity cases.

Conclusion: The limiting instability mode for the NPM is riser instability, also called NPM natural circulation instability. Section 5.0 describes models used to analyze this instability. Section 8.0 and 9.0 present the results for various representative operating conditions and sensitivity cases using these models.

4.4 Phenomena Identification and Ranking Table

This section identifies and ranks the parameters and phenomena that are needed to construct a working model for stability analysis. This identification is presented in a table form in Table 4-1. The ranking is labeled H, M, L, or N for High, Medium, Low, and Not Applicable, respectively. The "Not Applicable" category is reserved for phenomena that were thought from past experience of other nuclear systems to be applicable and of some importance, but were found not to apply to the NPM, nor to the case in which the excitation of that phenomenon is preceded by another more important phenomenon and therefore not limiting. The knowledge level for each item is included in parentheses, where (1) indicates deficient knowledge and (4) indicates well characterized. Phenomena or parameters ranking H(1) are of most concern and L(4) are of least concern.

Table 4-1 forms the basis for constructing the analytical model described in Section 5.0. Section 10.1 examines the highly-ranked phenomena to show that they are accounted for adequately in the evaluation methodology.

Table 4-1. Phenomena Identification and Ranking Table

{{

}}2(a),(c)

{{

}}2(a),(c)

{{

}}2(a),(c)

5.0 Theory and Model Description of the PIM Code

5.1 Background

The objective of the PIM code is to simulate the dynamics of the flow in the NPM coolant loop with special attention to optimal resolution of its stability. The extensive experience in the field of BWR stability analysis, both numerical and first principle understanding, has been utilized in addressing the new problem of single-phase natural circulation stability that is unique to the NPM. The guiding principle in designing the PIM code is maintaining simplicity, which is essential to the fidelity of stability analysis, while avoiding over simplifications that would sacrifice the level of details needed to ensure the applicability of the model to the actual reactor design and the important phenomena that were identified prior to the stability work.

Based on industry experience, including work in national laboratories and universities in the United States and abroad, it was found that a successful algorithm for thermal-hydraulic stability is that of the RAMONA series of codes (References 12.1.19 and 12.1.20). The PIM code relies on the published description of the theory and numerical methods of RAMONA, but is not a direct derivative of the coding, which has been developed independently to address the geometry and specific needs of the NPM. The main advantage of the RAMONA-type algorithm is the absence, or insignificance, of numerical damping that affects other time-domain codes, and requires extensive studies and adjustments before they can be successfully benchmarked and reliably used.

Even though frequency-domain methods in general are not affected by the numerical damping problem as much as some time-domain methods, frequency-domain methods have not been selected because they require linearization of the governing equations. While linearization is accurate for small perturbations and properly identifies the decay ratio and the conditions at the onset of instability, fundamentally frequency domain methods are not suitable to analyze the stability of a highly-nonlinear system, such as a natural circulation loop. A linearized model would not be able to discover the importance of nonlinearities that may be manifested at relatively small perturbation amplitudes. Fortunately, the RAMONA-type algorithm is capable of representing the nonlinear interactions inherent in the natural circulation flow under study.

5.2 Assumptions and Limitations

The modeling in PIM is by necessity an approximation of the actual RPV and the flow therein. The approximations are founded on basic assumptions regarding the geometry and the representation of the flow fields and various interactions and feedback mechanisms. Listing these assumptions and approximations is useful to put the results in the right perspective and guide the assessment of uncertainties and accuracy of the stability parameters. The major assumptions of the PIM code formulation are listed below with the corresponding justification and engineering judgment regarding their impact on the stability results. More details about modeling assumptions and their impact and justifications are given in the respective sections describing various submodels:

1. The flow around the primary loop of the NPM is one-dimensional where the flow area varies along the flow path. This one-dimensional approximation is understandable given the geometry of the loop where the flow direction is streamlined along the length of the various components, core, riser, and downcomer. Two-dimensional effects would be manifest, for example, if there were pumps distributed azimuthally around the downcomer where not all of the pumps may be running. Two-dimensional effects would also be manifested if there were multiple independent SGs where the SG in one region is operated differently from other regions. The effects are not possible in the NPM.
2. The flow in the core is represented by a single channel and coolant flow in the reflector, control rod guide tubes, and instrument tubes is included in the active core flow. This assumption is reasonable given that the individual fuel assemblies are not confined in canisters or channels like those of BWR fuel assemblies. The alternative approximation of several parallel channels to represent the flow in the core would neglect crossflow, which is not obstructed in PWR cores. The extent of this approximation is neglecting the effect of planar power distribution in the core on the generation of subcooled voids that may survive, enter the riser section, and affect the density head. {{

}}$^{2(a),(c),ECI}$

3. Power generation in the core is represented by a point kinetics model. Accordingly, the axial power shape is invariant, which is a reasonable approximation given that only minimal subcooled voiding is possible.
4. {{

}}2(a),(c),ECI

5. The flow in the primary coolant loop is modeled as non-equilibrium two-phase flow in which a drift flux formulation accounts for mechanical (velocity) differences between the liquid phase and the vapor phase if vapor exists. Thermal non-equilibrium allows the liquid to be in a subcooled, saturated, or superheated state, but the vapor is restricted to the saturation state. Closing relations governing mass, momentum, and energy exchange between the phases and the solid structures are adaptations from commonly used correlations. The algorithms do not account for the possibility of reverse flow.
6. The flow in the secondary side of the SG is modeled {{

}}2(a),(c),ECI

7. The pressurizer is not modeled. Pressure is specified by input and the dependence of thermodynamic properties on pressure is uniform. This approximation implies that pressure waves cannot be simulated where the sound speed is infinite. Given the long transport times for fluid transit around the primary coolant loop and the low frequency of the oscillations following any perturbation of the steady state, the impact of this approximation on the stability calculation is negligible. {{

}}2(a),(c)

8. A simplified model for ambient heat losses along the downcomer to the containment vessel and reactor provides representative estimates for this small effect on natural circulation driving head, which has some contribution at low power conditions. The reason it is included is to improve consistency with plant operating condition estimates for SG exit conditions. Not including this small effect would result in hotter steam exit conditions than plant operating estimates. Additionally, it is useful to include it for module heatup calculations when the SG is not online and the system is being heated by the CVCS heater.
9. The solid structures within the RPV, except the fuel rods in the core and the SG tubes, are assumed to have no heat exchange with the circulating fluid. This assumption essentially neglects the thermal inertia of the RPV, so it is conservative.

This assumption includes the effect of heat transfer from the riser or core into the cold leg, which is similarly conservative.

10. The total core thermal power, flow rate, pressure, and inlet temperature are specified initial conditions for the primary coolant and SG secondary side. The specified conditions are based on plant performance operational predictions associated with plant design activities, or as chosen for sensitivity studies. Preserving these specified conditions means that the SG total heat transfer performance is effectively specified. Therefore, the SG heat transfer modeling performed here defines the relative heat transfer profile of the SG and requires capabilities to establish the specified initial conditions.

The following limitations of usage stemming from the theory and modelling apply:

1. Prediction of large oscillation amplitudes that produce reverse flow in the primary system is not supported.
2. Prediction of effects of post-critical heat flux (CHF) heat transfer on fuel rods in the core is not supported.
3. Evaluation of the effects of loss-of-coolant accident is not supported.

5.3 Conventions

The PIM code is programmed to receive input and give output in SI units and dimensional internal variables use SI units. Units of meters, kilograms, and seconds are consistent throughout the coding, except selected special modeling. The working unit for temperature is Celsius. The unit of pressure and pressure drop is Pascal. Calculations such as change in pressure due to a form loss use this unit, but more convenient units of bar or millibar are used in some cases to apply a sensible scale. Primary and secondary pressures are input with units of bar and this unit is used for system pressure within the coding.

Theoretical discussions provided in this report utilize the above units, where departures from the standard values are indicated by defining the units of a variable appropriately.

5.4 Geometry Representation

Figure 5-1 illustrates the geometry representation of the NPM pressure vessel for the numerical simulation. The primary coolant loop is a one-dimensional flow path with generally varying cross-section area along the flow direction. A heated section at the bottom of the riser represents the core. A one-dimensional pipe, also of generally varying cross-section area, represents the cold leg annulus. The helical coils of the SG fill part of the cold leg volume and heat is exchanged between the downward flow in the primary coolant loop and the secondary side (inside of the helical heat exchanger coil tubes). The dashed line represents a pressure boundary condition that is imposed by the pressurizer.

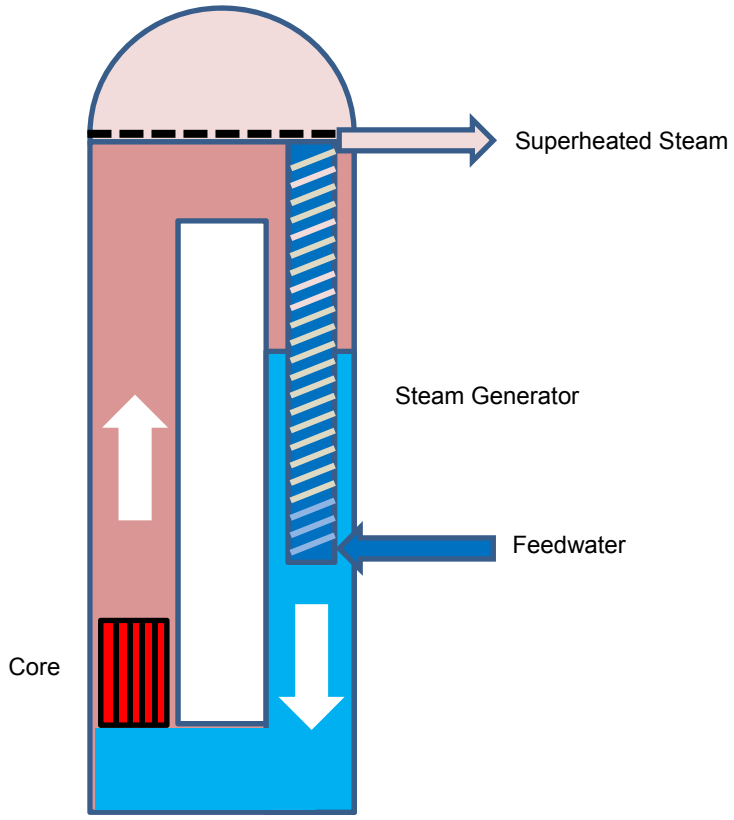

Figure 5-1: Illustration of the Geometry Representation of the NuScale Power Module

5.5 Thermal-hydraulic Model

The thermal-hydraulic model of the primary coolant loop is constructed by applying non-homogeneous, non-equilibrium, time-dependent mass, momentum, and energy balance equations for two-phase flow to the one-dimensional finite volume geometry representing the NPM. The geometry of the primary coolant loop is represented by a one-dimensional closed loop that is divided to N nodes or volumes of varying length and cross-section area. {{

}}$^{2(a),(c),ECI}$

In the next subsections, the time-dependent conservation equations are written and adapted to the one-dimensional finite volume geometry. Constitutive relations and boundary conditions are also presented.

5.5.1 Conservation Equations

5.5.1.1 Mass Balance

The differential form of the vapor mass balance is written as

$$\frac{\partial}{\partial t}\left(\alpha\rho_g\right)+\nabla\cdot\left(\alpha\rho_g\vec{v}_g\right)=\Gamma''' \qquad \text{Eq. 5-1}$$

where

t = time
α = void fraction
ρ_g = vapor density (a function of local conditions at the reference pressure)
$\vec{v}_g$ = vapor velocity (vector)
Γ''' = rate of vapor mass generated per unit volume

Integrating over the volume of a finite control volume and applying Gauss's theorem, considering that the flow velocity is perpendicular to the cross-section area of the control volume, the mass balance equation becomes

$$\frac{\partial}{\partial t}\left(V\alpha\rho_g\right)_n+\left(A\alpha\rho_g v_g\right)_{n+1/2}-\left(A\alpha\rho_g v_g\right)_{n-1/2}=\left(\Gamma'''V\right)_n \qquad \text{Eq. 5-2}$$

where

A = cross-section area
V = volume

and the subscript n refers to the average or bulk of the control volume, and $n\pm1/2$ refers to the inlet and outlet boundaries of the control volume, respectively.

The differential form of the one-dimensional vapor mass conservation equation can be obtained for a generally varying cross-section area along the flow direction, $A(z)$, by considering an infinitesimal control volume and substituting $V=A(z)dz$ in Eq. 5-2 to get

$$\frac{\partial}{\partial t}\left(\alpha\rho_g\right)+\frac{1}{A}\frac{\partial}{\partial z}\left(A\alpha\rho_g v_g\right)=\Gamma''' \qquad \text{Eq. 5-3}$$

The form of Eq. 5-3, where the divergence term is replaced with a one-dimensional spatial derivative with the cross-section area included in the differential and the term is divided by the cross-section area, is valid for the transport of other conserved quantities such as energy and momentum. {{

}}[2(a),(c)]

{{

}}2(a),(c)

The vapor mass, M, in the control volume, n, is obtained from

$$M_n = \left(V \alpha \rho_g\right)_n \qquad \text{Eq. 5-4}$$

and the vapor mass flow rate $\dot{m}$ at a given boundary from

$$\dot{m}_{g,n-1/2} = \left(A \alpha \rho_g v_g\right)_{n-1/2} \qquad \text{Eq. 5-5}$$

Substituting the vapor mass and vapor mass flow rate, and observing that the vapor mass in the control volume is a function of time only, the partial time derivative is replaced by a total time derivative gives {{

}}2(a),(c)

5.5.1.2 Energy Balance

An energy balance equation for the vapor phase is not required because the vapor is assumed to be in the saturation state in the reactor primary coolant loop. A single energy equation is required to account for energy conservation. For the RAMONA code, a mixture-energy equation is used, while here the equivalent option of liquid energy balance is used.

For the liquid phase, the energy balance can be derived using the form of the mass balance, and modifying the parameters to account for the energy carried by the mass flow and including terms accounting for the heat of vaporization and heat transfer through the wall of the control volume. Thus, for control volume, n, {{

}}$^{2(a),(c)}$

{{

}}2(a),(c)

5.5.1.3 Momentum Balance

The momentum balance equation for the two-phase mixture in the one-dimensional differential form is given as (Reference 12.1.21)

$$\frac{\partial G}{\partial t}+\frac{1}{A}\frac{\partial}{\partial z}\left(A\left(\alpha\rho_g v_g^2+\left(1-\alpha\right)\rho_l v_l^2\right)\right)=-\frac{\partial P}{\partial z}-\frac{\partial F}{\partial z}+\vec{g}\cdot\hat{z}\left(\alpha\rho_g+\left(1-\alpha\right)\rho_l\right) \qquad \text{Eq. 5-13}$$

where the mass flux G is obtained from

$$G=\alpha\rho_g v_g+\left(1-\alpha\right)\rho_l v_l \qquad \text{Eq. 5-14}$$

is the two-phase mixture mass flux, and

P = pressure
F = wall and local friction function
$\vec{g}$ = gravitational acceleration vector
$\hat{z}$ = unit vector pointing to the flow direction

Notice that $\vec{g}\cdot\hat{z}=\pm g$ for downflow and upflow respectively, where the gravitational constant g is positive.

{{

}}2(a),(c)

{{

}}[2(a),(c)]

{{

}}[2(a),(c)]

{{

}}2(a),(c)

{{

}}[2(a),(c)]

{{

}}[2(a),(c)]

To sum up, the finite volume one-dimensional two-phase flow dynamic model differential equations are {{

}}[2(a),(c)]

- {{

}}2(a),(c)

5.5.2 Numerical Solution Procedure

This section describes the solution technique, followed by a presentation of the closing relations and correlations in the following section.

The ordinary differential equations representing the flow transient are solved by a first order finite difference approximation of the time derivatives and the equations are solved by the explicit Euler method. Thus, Eq. 5-7, Eq. 5-8, Eq. 5-12, and Eq. 5-35, respectively, are approximated as {{

}}2(a),(c)

In the steady-state initialization, the void fraction is obtained directly for a given control volume from the steam quality as

$$\alpha = \frac{\left(\frac{\rho_f}{\rho_g}\right)x}{C_o\left(1+\left(\frac{\rho_f}{\rho_g}-1\right)x\right)+\frac{V_{gj}\rho_f A}{\dot{m}}} \qquad \text{Eq. 5-40}$$

where

x	=	flow quality
ρ_f	=	saturated liquid density
ρ_g	=	saturated vapor density
A	=	flow area
$\dot{m}$	=	mass flow rate
C_0	=	drift flux concentration parameter
V_{gj}	=	drift flux velocity

The steady-state solution is obtained by a modified null transient for which the system of differential equations is solved by time integration starting from an initial guess of the flow field. The solution method differs from a true null transient method because the true null transient does not converge in the important case of a physically unstable system, a situation that is not known *a priori*. {{

}}2(a),(c)

The void fraction during transients, including a null transient, is obtained from the vapor mass in the control volume, which is a state variable. Thus,

$$\alpha = \frac{M_g}{\rho_g V} \qquad \text{Eq. 5-41}$$

In the modified null transient, {{

}}2(a),(c)

{{

}}2(a),(c)

In the above solution description, closing relations including the vapor generation and condensation, drift flux correlations, pressure drop correlations, and the heat source/sink from heat transfer in the core and the SG, are described separately in subsequent sections.

5.5.3 Steam Generator Model

The PIM code uses a simplified model of the inclined, helically-coiled SG heat transfer performance in which the secondary mass flow rate and feedwater inlet temperature are specified for all nodes through initial conditions and transient boundary conditions. No momentum solution is used and a simplified energy equation is used based on incremental energy addition from the primary system through the SG tubes. Accordingly, the flow enthalpy at the exit of an SG tube control volume (node) is calculated from

$$h_{n+1} = h_n + \dot{Q}_n \qquad \text{Eq. 5-43}$$

where

h_n = flow enthalpy at a SG node boundary
$\dot{Q}_n$ = rate of heat transfer through the tube wall for the node
n = subscript indicating SG node number

Note that the geometry of the nodalization of the primary and secondary flow paths assigns correspondence between the two such that energy is exchanged across the SG tube wall between a single primary node and a single corresponding secondary node.

The purpose of the SG model is to provide a representative distribution of primary-side fluid density in the vicinity of the SG by predicting axial evolution of total heat removal to the secondary fluid along the axial length of the SG. The code user specifies {{

}}2(a),(c)

Within the structure of the analysis model described in this section, the SG model encompasses modeling of the secondary fluid conditions, conduction through the SG tubes, and heat transfer at the primary-side and secondary-side tube surfaces. The SG

is incorporated into the analysis model via the rate of heat removal from each primary node in the region of the SG, variable $\dot{Q}_n$ of the energy balance shown in Eq. 5-9. At each time step, the current-time primary temperature and flow rate associated with each node of the SG is used {{

}}2(a),(c),ECI

A single column of nodes, assuming the mass flow in the SG tubes is the same in each, represents fluid in the secondary side of the SG. Total flow area within the SG tubes and average tube length are used in the modeling. {{

}}2(a),(c),ECI The heat transfer area of primary and secondary control volumes associated with thermal conduction through the tubes and heat transfer on the surfaces of the tubes is determined by the dimensions of the inclined helical geometry of the SG tubes.

{{

}}2(a),(c) The enthalpy in each node of the secondary is used to determine the fluid temperature and heat transfer regime associated with heat transfer on the inside of the SG tubes.

As noted in the assumptions and limitations described in Section 5.2, the total heat transfer performance of the SG is effectively defined {{

}}2(a),(c)

The cylindrical conduction equation for the SG tube walls is solved consistent with the description in Section 5.6.3.

The primary and secondary sides interact by exchanging heat through the SG tube walls. Conditions for forced convective heat transfer on the primary side use single-phase correlations appropriate for crossflow heat transfer on the exterior of the tubes (two-phase models are not included). The modeling is consistent with the NRELAP5 heat transfer package for primary-side crossflow heat transfer and has the following form,

$$Nu = C\,Re^{n}\,Pr^{m} \qquad \text{Eq. 5-44}$$

where

Nu = Nusselt number
Re = Reynolds number
Pr = Prandtl number

{{

}}2(a),(c)

Heat transfer modeling on the secondary side (inside the SG tubes) covers the entire range from subcooled single-phase liquid to superheated vapor. The Dittus-Boelter correlation is used for single-phase liquid and vapor forced convection heat transfer from Eq. (8.59) of Reference 12.1.24

$$Nu = 0.023\ Re^{0.8}\ Pr^{0.4} \qquad \text{Eq. 5-45}$$

where the Reynolds and Nusselt numbers are based on a characteristic length taken as the tubes' inner diameter.

Boiling heat transfer is modeled with the form of the Chen correlation extended to subcooled boiling as proposed by Collier, Eq. (12-33) of Reference 12.1.25. Accordingly, the heat flux is obtained from

$$q'' = h_{NB}\left(T_w - T_{sat}\right) + h_c\left(T_w - T_{bulk}\right) \qquad \text{Eq. 5-46}$$

where

T_w = wall temperature
T_{sat} = fluid saturation temperature
T_{bulk} = fluid bulk temperature

The nucleate boiling heat transfer coefficient, h_{NB}, is as shown in Eq. (12-31) and the convective term, h_c, is shown in Eq. (12-29) of Reference 12.1.25.

Laminar and turbulent natural convection contributions are computed in addition to the forced convection effects described above. The forced and natural convection effects

{{

}}2(a),(c)

5.5.4 Ambient Heat Losses

A simplified model is used to optionally account for ambient heat losses from the primary vessel to the containment and into the reactor pool. This heat loss reduces the amount of heat passing through the SGs and is consistent with heat balance calculations. The model is incorporated via the variable $\dot{Q}_n$ of the energy balance shown in Eq. 5-9 for nodes associated with the downcomer. Ambient losses are added to the SG heat rate for nodes in which both effects are present.

At each time step, the current-time primary temperature of each node of the downcomer is used to calculate a new-time nodal heat removal rate from the primary. The ambient heat rate for node n is calculated from

$$\dot{Q}_n = h_{amb}\,\pi\,D_{vess,n}\,\Delta z_n\,\left(T_{bulk.n} - T_{amb}\right) \qquad \text{Eq. 5-47}$$

where

h_{amb} = ambient heat transfer coefficient
$D_{vess,n}$ = user-input vessel inner diameter
T_{amb} . = user-input ambient reactor pool temperature

The ambient heat transfer coefficient is empirically determined to approximate ambient heat losses. It includes effects of conduction through the reactor and containment vessels, thermal radiation between the vessel wall inside the containment volume, and surface heat transfer rates. The heat transfer coefficient is as follows. {{

}}2(a),(c)

5.5.5 Chemical and Volume Control System Model

Modeling of the CVCS is provided for two purposes. First, during at-power operations the model simulates heat losses associated with cooling water to an acceptable temperature for passing through the chemical exchange systems. This heat loss reduces the amount of heat passing through the SGs and is consistent with heat balance calculations. Second, the model is necessary to perform module heatup calculations, where a heater in the CVCS supplies energy the primary system coolant and induces primary coolant flow.

In PIM, the CVCS is modeled by withdrawing letdown flow from a user-specified node in the downcomer at the local node conditions, passing the extracted fluid through the CVCS heaters and pumps, and returning charging flow to a user-specified node in the riser. The fluid mass and energy are added to the node. {{

}}2(a),(c)

Modeling of the regenerative and non-regenerative heat exchangers is performed using a total {{ }}2(a),(c)

{{

}}[2(a),(c)]

5.5.6 Closing Relations

The system of equations derived from the differential form of the mass and momentum and energy balance require additional algebraic relations. These closing relations include the following:

- fluid properties - thermodynamic state equations and transport properties
- pressure drop correlations including single-phase friction and two-phase multipliers
- form losses including two-phase multipliers
- drift flux parameters
- evaporation and condensation rates
- heat transfer coefficients

Except for heat transfer coefficients, the relations are presented in the following sections. Heat transfer related to the SG is described in Section 5.5.3 and heat transfer related to the core is described in Section 5.6.

5.5.6.1 Fluid Properties

Fluid properties are based on curve fits of the necessary fluid properties over the expected range of analysis. Fits are verified by comparing to an implementation of the International Association of the Properties of Water and Steam (IAPWS), 1995 version described in Reference 12.1.26. Key properties necessary in PIM are described below.

The following saturation properties are calculated as functions of pressure:

- saturation temperature (degrees-C)
- liquid density (kg/m^3)
- vapor density (kg/m^3)
- liquid enthalpy (J/kg)
- heat of vaporization (J/kg)
- liquid specific heat (J/kg-K)
- vapor specific heat (J/kg-K)

The following saturation properties are calculated as functions of saturation temperature:

- liquid viscosity (kg/m-s or Pa-s)

- vapor viscosity (kg/m-s or Pa-s)
- liquid conductivity (W/m-K)
- vapor conductivity (W/m-K)
- surface tension (N/m)

The following subcooled liquid and superheated vapor properties are calculated:

- liquid temperature from liquid enthalpy (degrees-C), where the input liquid enthalpy is referenced to saturation enthalpy
- liquid density from pressure and enthalpy (kg/m^3)
- vapor temperature from pressure and vapor enthalpy (degrees-C)
- vapor Prandtl number from pressure and temperature (-)

Other properties, such as liquid Prandtl number, are derived from the appropriate functions. Inverse properties for liquid enthalpy as a function of liquid temperature are determined {{

}}$^{2(a),(c)}$

5.5.6.2 Frictional Pressure Drop

Frictional pressure drop, $\Delta P_{fric,n}$, across a node (control volume) , n, is calculated using standard techniques for two-phase conditions and is based on the single-phase Darcy friction factor formulation. Dropping the subscript indicating the node to simplify notation gives

$$\Delta P_{fric} = \frac{f_m \, \Delta z}{D_H} \, \frac{\dot{m}^2}{2\rho_l A^2} \qquad \text{Eq. 5-49}$$

where

f_m	=	friction factor (for single-phase or two-phase flow)
D_H	=	hydraulic diameter
Δz	=	length of node (control volume)
A	=	flow area

The friction factor is correlated as function of Reynolds number for single-phase flow, and a quality-weighted function of liquid and vapor friction factors for two-phase flow. The liquid and vapor Reynolds numbers are calculated as

$$\mathrm{Re}_{1\phi} = \frac{\dot{m}\, D_H}{\mu_{1\phi}\, A} \qquad \text{Eq. 5-50}$$

where

$\dot{m}$ mass flow rate
D_H hydraulic diameter of the pipe or rod bundle
$\mu_{1\phi}$ dynamic viscosity of the liquid or vapor
A flow area

The subscript 1ϕ stands for either l (liquid) or v (vapor).

5.5.6.2.1 Single-Phase Friction Factor

A single-phase friction factor model is described that has more complexity than that described in Reference 12.1.27, which addresses only the smooth-tube formulation of Blasius for turbulent flow and does not address the transition region between laminar and turbulent flow. Here, an explicit form of the Colebrook equation (Reference 12.1.28) for friction factor as function of Reynolds number and relative roughness is used along with a transition ramping model. The basis for the friction factor model described here is Section 3.3.8.6 of Reference 12.1.29.

The single-phase friction coefficient, $f_{1\phi}$, can be calculated as a function of the phasic Reynolds number in Eq. 5-50 for three different regions as follows:

$$f_{1\phi} = \begin{cases} f_{L,1\phi} & \text{laminar region} & \mathrm{Re}_{1\phi} \le \mathrm{Re}_{low} \\ f_{\mathrm{Tran},1\phi} & \text{transition region} & \mathrm{Re}_{low} < \mathrm{Re}_{1\phi} \le \mathrm{Re}_{high} \\ f_{T,1\phi} & \text{turbulent region} & \mathrm{Re}_{high} < \mathrm{Re}_{1\phi} \end{cases} \qquad \text{Eq. 5-51}$$

where

Re_{low} = Reynolds number lower limit for the laminar-to-turbulent transition region
Re_{high} = Reynolds number upper limit for the laminar-to-turbulent transition region

The transition from laminar to turbulent regimes is consistent with Reference 12.1.29. The value for these limits is user-input. The values described in Reference 12.1.29 are 2200 and 3000, respectively. The friction factor in the transition region is obtained by {{

}}$^{2(a),(c)}$

{{

}}2(a),(c)

5.5.6.2.2 Two-Phase Friction Factor

With single-phase friction factors evaluated based on liquid and vapor properties, the Reference 12.1.27 approach is used to model the two-phase transition between these conditions.

The single-phase friction factors are obtained from Eq. 5-51. {{

}}2(a),(c)

5.5.6.3 Pressure Drop for Local Form Losses

The generally two-phase form loss coefficient needed for evaluating pressure drop in Eq. 5-32 is correlated as function of the mixture Reynolds number. The latter is defined from

$$\mathrm{Re}_{2\phi} = \frac{\dot{m}\, D_H}{\mu_m\, A} \qquad \text{Eq. 5-57}$$

where the mixture viscosity is obtained from a quality-weighted interpolation of liquid and vapor viscosities [Cichitti et al. relation shown in Eq. (11-80b) of Reference 12.1.25] as

$$\mu_m = x\mu_v + (1-x)\,\mu_l \qquad \text{Eq. 5-58}$$

The loss coefficient as a function of the two-phase Reynolds number in Eq. 5-57 takes the form

$$\xi_{loc} = \left(\frac{A}{A_{ref}}\right)^2 \left[a\left(\frac{A}{A_{ref}}\right)^b \mathrm{Re}_{2\phi}^b + c \right] \qquad \text{Eq. 5-59}$$

where the coefficients a, b, and c are user-input along with a reference area A_{ref} associated with the loss coefficients.

5.5.6.4 Drift Flux Parameters

The drift flux parameters used in formulating the flow equations are the concentration parameter, C_0 , and the drift velocity, V_{gj} . Homogeneous flow conditions can be imposed by specifying $C_0 = 1$ and $V_{gj} = 0$.

For non-homogeneous flow, the values of the drift flux parameters are user-input. A correlation for the drift flux parameters is obtained from Eq. (3.10) of Reference 12.1.30. Accordingly, {{

}}2(a),(c)

5.5.6.5 Evaporation and Condensation

The correlation for phase change (evaporation and condensation) is adapted {{

}}[2(a),(c)]

{{

}}2(a),(c)

The latent heat and the reference saturation enthalpy vary with pressure. While the pressure is assumed to be uniform for all other considerations to avoid tracking acoustic waves at the expense of density wave stability fidelity, an exception is made for the vapor generation model. By adjusting the pressure due to static head, the physically correct enthalpies are used and flashing in the riser can be calculated.

5.6 Core Modeling

5.6.1 Neutron Kinetics

A point neutron kinetics model represents the dynamics of the power generated in the core with {{
}}2(a),(c) These assumptions and simplifications are suitable to the simulation of a small PWR core. The three-dimensional power distribution changes during transients originate in large local reactivity variations, such as control rod motion, significant boiling, or out-of-phase density wave instabilities, which may occur in a large core. These phenomena are not important in the stability calculations of the NPM.

The time scale of reactivity changes corresponds to the time scale of flow and temperature changes caused by possible flow oscillations. This time scale is larger than that of the prompt neutrons. Prompt neutron criticality is not possible as a consequence of thermal-hydraulic oscillations. This condition makes the prompt jump approximation physically suitable, but not necessary. The prompt jump approximation is not used because it would result in mathematical singularities in the case of applying the code outside its originally intended scope where large reactivity insertion occurs.

In the point kinetics approximation, the neutron flux distribution remains invariant during a transient while the magnitude of the neutron flux changes with time. The same assumption is applicable to the distributions of the delayed neutron precursors and the generated fission power. Thus, following Reference 12.1.12, the point kinetics equations are given as

$$\Lambda \frac{d\Phi}{dt} = \beta\left(\rho - 1\right)\Phi + \lambda C \qquad \text{Eq. 5-67}$$

$$\frac{dC}{dt} = \beta\Phi - \lambda C \qquad \text{Eq. 5-68}$$

where

Φ	=	dimensionless amplitude of the neutron flux, or equivalently power
C	=	amplitude of the delayed neutron precursor concentration
ρ	=	reactivity in dollars
Λ	=	prompt neutron generation, sec
β	=	delayed neutron fraction
λ	=	decay constant of the delayed neutron precursors, sec^{-1}

The time derivatives are approximated using first order finite differencing and an {{

}}2(a), (c)

{{

}}2(a),(c)

5.6.1.1 Doppler Reactivity Calculation

Fuel temperature reactivity feedback is calculated from the effective fuel temperature for Doppler reactivity (variable $T_{Doppler}$) shown in Eq. 5-102 of Section 5.6.4.4. This is a single temperature representing the average fuel temperature in the core. The fuel temperature reactivity feedback accounts for effects, such as temperature dependence of resonance integrals, in a manner similar to Eq. (14-34) of Reference 12.1.31 and is calculated from

$$\Delta k_{Dopp} = M_{Dopp} C_{Dopp} \left[\sqrt{T_{Doppler,0} + 273.15} - \sqrt{T_{Doppler} + 273.15} \right] \qquad \text{Eq. 5-76}$$

where

Δk_{Dopp} = change in multiplication factor due to the Doppler effect
$T_{Doppler}$ = effective fuel temperature for Doppler reactivity (degrees-C)
$T_{Doppler,0}$ = initial temperature at start of the transient (degrees-C)
C_{Dopp} = Doppler coefficient
M_{Dopp} = user specified Doppler coefficient multiplier

The Doppler coefficient is exposure-dependent and has a form consistent with Eq. (14-36) of Reference 12.1.31. The relative cycle exposure is used to {{

}}2(a),(c)

{{

}}2(a),(c)

5.6.1.2 Moderator Reactivity Calculation

The moderator reactivity feedback is accounted for based on change {{

}}2(a),(c)

{{

}}2(a),(c)

Notice that at cold conditions in which the density is relatively high, negative moderator *density* (positive moderator *temperature*) reactivity feedback is possible at low exposure where the boron content is relatively high. This phenomenon is equivalent to a positive MTC.

{{

}}2(a),(c),ECI

The total density reactivity feedback is calculated by summing over all nodes in the core by node volume and neutron-flux squared weighting. The neutron flux distribution is taken as the axial power distribution provided as a user input.

$$\Delta k_{MD} = \frac{\sum_{n=1}^{N} \Delta k_{MD,n} \left(\Delta z_n \phi_n \right)^2}{\sum_{n=1}^{N} \left(\Delta z_n \phi_n \right)^2} \qquad \text{Eq. 5-81}$$

where

Δk_{MD} = change in multiplication factor in the core due to moderator density change

Δz_n = height of node n (total number of core nodes is N)

ϕ_n = normalized neutron flux/power profile from input for core nodes, n

5.6.1.3 Net Reactivity Calculation

The net reactivity feedback is calculated by the sum of change in multiplication factor due to the Doppler effect and moderator density change. The reactivity in dollar units is then obtained by dividing by the delayed neutron fraction and used to drive the point kinetics equations.

The user can modify the reactivity feedback by adding or multiplying the calculated reactivity for the purpose of sensitivity analysis as indicated in the last sections. External reactivity can be added as a user-specified forcing function. This functionality allows the simulation of boron concentration changes and control rod movement as functions of time.

5.6.2 Decay Heat

The decay heat is maintained at a constant thermal power throughout a calculation and is input by the user as a percentage of the initial thermal power. This approach is taken because the time response of decay heat is larger than an oscillation period and it allows direct access to initial decay heat load for sensitivity studies.

5.6.3 Cylindrical Heat Conduction

The heat equation for transient conduction in cylindrical coordinates with constant properties and no internal heat generation for the SG tubes and fuel cladding is

$$\rho c_p \frac{\partial T}{\partial t} = k \frac{1}{r} \frac{\partial}{\partial r}\left(r \frac{\partial T}{\partial r} \right) \qquad \text{Eq. 5-82}$$

where

T	=	temperature
r	=	radial position from tube center
ρ	=	density
k	=	thermal conductivity
c_p	=	specific heat

This equation can be written in finite difference form and solved implicitly for temperature at chosen radial mesh points.

Radial discretization is accomplished by dividing the cylindrical cross section into M-1 shells, that is M surfaces, including the inner and outer surfaces. The thickness of the shells is uniform. Thus,

$$\Delta r = \frac{r_s - r_i}{M - 1} \qquad \text{Eq. 5-83}$$

where

$r_s = r_M$ = outer surface radius
$r_i = r_1$ = inner surface radius

Figure 5-2 illustrates the discretization scheme.

The implicit finite-difference equations for interior nodes, $m = 2, 3, ..., M-1$, can be expressed as

$$\frac{\rho C_p}{k}\frac{T_m - T_m^{(old)}}{\delta t} = \frac{\left(r_m + \frac{\Delta r}{2}\right)\left(\frac{T_{m+1} - T_m}{\Delta r}\right) - \left(r_m - \frac{\Delta r}{2}\right)\left(\frac{T_m - T_{m-1}}{\Delta r}\right)}{r_m \Delta r} \qquad \text{Eq. 5-84}$$

where the superscript (*old*) refers to the previous time step value, and

δt = time step
r_m = shell radius at node m

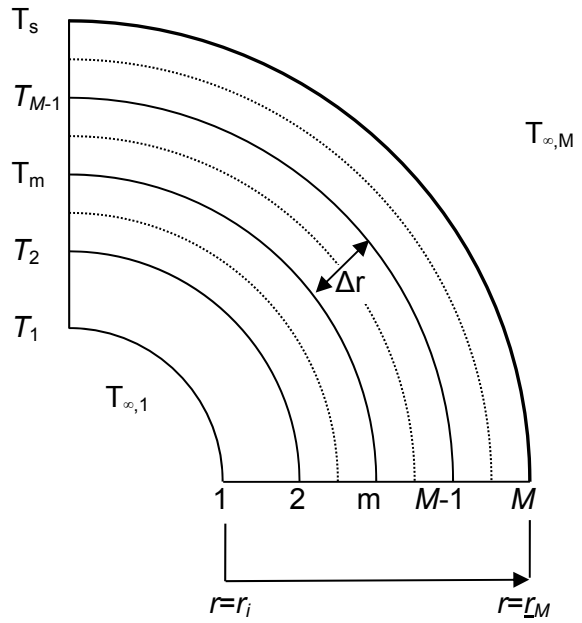

Figure 5-2. Cylindrical conduction nodalization

The outer surface (node M) is exposed to fluid contact and is subject to a convective boundary condition,

$$-k\frac{\partial T}{\partial r} = h\left(T_M - T_\infty\right) \qquad \text{Eq. 5-85}$$

that leads to the finite difference form at the outer edge,

$$\frac{\rho C_p}{k}\frac{T_M - T_M^{(old)}}{\delta t} = \frac{r_M \frac{h}{k}\left(T_{\infty,M} - T_M\right) - \left(r_M - \frac{\Delta r}{2}\right)\left(\frac{T_M - T_{M-1}}{\Delta r}\right)}{r_M \Delta r/2} \qquad \text{Eq. 5-86}$$

The equivalent equation for the inner surface node at $m=1$ is similarly written as

$$\frac{\rho C_p}{k}\frac{T_1 - T_1^{(old)}}{\delta t} = \frac{\left(r_1 + \frac{\Delta r}{2}\right)\left(\frac{T_2 - T_1}{\Delta r}\right) - r_1 \frac{h}{k}\left(T_{\infty,1} - T_1\right)}{r_1 \Delta r/2} \qquad \text{Eq. 5-87}$$

Equations Eq. 5-84, Eq. 5-86, and Eq. 5-87 can be rearranged in matrix form for old- and new-time temperatures and solved in a standard matrix solver. Material properties of the SG tubes and clad are addressed in Section 5.7. Heat transfer coefficients are determined for the SG as described in Section 5.5.3 and for the fuel rods as described in Section 5.6.4.

5.6.4 Fuel Rod Heat Conduction

The calculations of the fission and decay heat generation are described in previous sections using a point kinetics model and user-input decay heat value. Most of the fission energy is deposited in the UO_2 pellets in the fuel rods, while a small percentage resulting from neutron slowing down and gamma absorption is deposited directly in the coolant.

The determination of the total heat source to the coolant requires performing the transient thermal conduction in the fuel pins for the heat transfer through the fuel pin cladding wall. In the steady state, all of the fission heat generated is equated to the heat source, but for transients the effects of heat capacity and finite thermal conductivity of the fuel pins result in a filtering effect in which the heat generated in the fuel pins is transferred to the coolant with a damping of amplitude and a time delay.

In addition to determining the total heat source to the coolant, an effective fuel temperature is necessary for use in fuel Doppler feedback to the point kinetics model, which requires a single effective temperature for the fuel pellets in the core.

Both of these objectives require a fuel rod model that accounts for the pellet, pellet-clad gap, cladding condition, and heat transfer from the clad surface to the coolant.

In performing these calculations, one single average pellet is analyzed to determine temperature and heat flux based on the core average power deposited in the fuel pellet, the core average coolant temperature, and the core inlet flow rate. Then, the total heat rate to the coolant is apportioned to the individual nodes of the core based on the input axial power profile. This single pellet model is a sufficient representation of the core for the slow (with respect to the thermal time constant through the pins) stability events.

5.6.4.1 Pellet Heat Transfer

An integral lumped parameter method is used to account for the heat conduction in the fuel pellets that accounts for the temperature dependence of the pellet conductivity. This approach is taken because the fuel temperature does not change quickly, and because the method {{

}}2(a),(c)

The power deposited in the pellets is related to the total fission energy calculated from the neutron point kinetics model as

$$Q_{pellet} = \left(1 - \varepsilon_D\right) Q_{fission} \qquad \text{Eq. 5-89}$$

where ε_D is the fraction of energy deposited directly in the coolant and has a typical value of 0.026 for a PWR.

Applying a finite difference approximation to the {{

}}2(a),(c)

{{

}}2(a),(c)

Section 5.7 addresses material properties of the fuel.

5.6.4.2 Cladding Heat Transfer Coefficient

Convective heat transfer from the surface of fuel rods is modeled for single-phase liquid water. The models are consistent with the subcooled heat transfer in the SG secondary described in Section 5.5.3, and mainly consists of the Dittus-Boelter equation for turbulent heated fluid from Eq. (8.59) of Reference 12.1.24

$$Nu_D = 0.023\ Re_D^{0.8}\ Pr^{0.4} \qquad \text{Eq. 5-93}$$

where D is the fuel assemblies hydraulic diameter. Natural convection from the tube surface and a convective lower limit are included, but they are generally unimportant in stability calculations.

5.6.4.3 Numerical Solution Procedure

Knowing the old-time heat flux from the pellet, the user input-heat transfer across the pellet-clad gap, and the old-time cladding inner temperature, the pellet surface temperature is calculated as the following:

$$T_{S,pellet} = T_{ci} + \frac{q_{pellet}}{A_{S,pellet}\ h_{gap}} \qquad \text{Eq. 5-94}$$

where

$T_{S,pellet}$ = pellet surface temperature
T_{ci} = clad inner surface temperature
$A_{S,pellet}$ = total pellet surface area
h_{gap} = pellet-clad gap heat transfer coefficient (user input)

This pellet surface temperature and pellet-clad gap heat transfer coefficient are in the cylindrical heat conduction equation along with the core average coolant temperature and cladding heat transfer coefficient to calculate updated cladding temperatures. The heat rate from the clad surface to the coolant is then calculated by

$$q_{clad} = -h_{clad}\, A_{clad} \left(T_{coolant} - T_{co} \right) \qquad \text{Eq. 5-95}$$

where

q_{clad} = heat rate from the clad surface to the coolant
h_{clad} = clad surface heat transfer coefficient
A_{clad} = total clad outer surface area
$T_{coolant}$ = coolant temperature
T_{co} = clad outer surface temperature

The total heat source to the coolant is thus obtained from

$$Q = \varepsilon_D Q_{fission} + q_{clad} \quad \text{Eq. 5-96}$$

Equation Eq. 5-96 is then used in conjunction with a specified power shape for the core to determine the rate of heat addition to each node in the region of the core, variable $\dot{Q}_n$ of the Energy Balance shown in Eq. 5-9.

5.6.4.4 Pellet Centerline and Average Temperature

Information on pellet temperature is necessary for determining the average pellet conductivity and fuel Doppler coefficient. Axial conduction is neglected, and the radial fuel conduction equation with assumed uniform volumetric heating is

$$-2\pi r k_f \frac{dT}{dr} = \pi r^2 q''' \quad \text{Eq. 5-97}$$

where

k_f = fuel pellet conductivity
T = temperature
q''' = volumetric heat generation rate for energy deposited in the fuel

The pellet conductivity dependence on temperature and burnup {{

}}2(a),(c)

{{

}}2(a),(c)

The average fuel temperature can then be estimated assuming uniform conductivity and heat source by

$$T_{avg} = \frac{1}{2}\left(T_0 + T_S\right) \qquad \text{Eq. 5-101}$$

Finally, the effective temperature used in fuel Doppler feedback to the point kinetics model includes surface importance weighting

$$T_{Doppler} = \omega T_{avg} + \left(1 - \omega\right) T_S \qquad \text{Eq. 5-102}$$

where

$T_{Doppler}$ = effective fuel temperature for Doppler reactivity

ω = temperature weighting factor, {{ }}2(a),(c)

5.6.5 Critical Heat Flux

The code analysis for the determination of the system stability does not result in any large oscillation magnitude and therefore does not require CHF calculation. However, for unstable cases that would result from inadvertent operation outside of the normal range, it is important to determine if the CHF is reached. For this purpose, the EPRI-1 correlation (Reference 12.1.32) is used to screen the results based on the relative change of the CHF ratio compared with its initial value.

{{

}}2(a),(c)

{{

}}2(a),(c)

The EPRI-1 correlation has the following basic form from Eq. (1) of Reference 12.1.32 (coefficients are indicated with a B instead of P for clarity relative to the reference). Note, other modified correlation forms to account for cold wall effects, grid spacers, and axial non-uniformities are proposed in Reference 12.1.32 and other references. These modifications are not applied here because the purpose is to predict trends in CHF

$$q''_{CHF} = \frac{A - x_{in}}{C + \left(x_L - x_{in}\right)/q''_L} \qquad \text{Eq. 5-103}$$

with the coefficients

$$A = B_1 p_r^{B_2} G^{\left(B_5 - B_7 p_r\right)} \qquad \text{Eq. 5-104}$$

$$C = B_3 p_r^{B_4} G^{\left(B_6 - B_8 p_r\right)} \qquad \text{Eq. 5-105}$$

where

q''_{CHF}	=	CHF (MBtu/hr-ft^2)
q''_L	=	local heat flux through cladding (MBtu/hr-ft^2)
$\overline{x}_{in}$	=	inlet equilibrium quality
$\overline{x}_L$	=	local equilibrium quality
G	=	mass flux (Mlbm/hr-ft^2)
p_r	=	reduced pressure (input pressure divided by critical pressure) $p_r = p/p_{crit}$
p_{crit}	=	critical pressure = 3206.2 psia (221.2 bar)
B_i	=	correlation coefficients for i=1, 2,..., 8 with the following values

$$B_1 = 0.5328 \qquad B_2 = 0.1212$$
$$B_3 = 1.6151 \qquad B_4 = 1.4066$$
$$B_5 = -0.3040 \qquad B_6 = 0.4843$$
$$B_7 = -0.3285 \qquad B_8 = -2.0749$$

Reference 12.1.32 describes the correlation parametric ranges to be pressure: 200 to 2450 psia, mass flux: 0.2 to 4.1 Mlb/hr-ft^2, quality: -0.25 to 0.75. Of these, the low flow range affects PIM modeling. {{

}}2(a),(c)

In implementing the CHF correlation within the scope of the one-dimensional core model of PIM, it is necessary to correctly account for radially non-uniform power (axial effects are accounted for by the user-specified axial power profile). The radial nonuniformity effect for the local hydraulic conditions {{

}}$^{2(a),(c)}$

The radial nonuniformity effect for the hot pin conditions at location L is accounted for by calculating the local heat flux through the cladding (a fraction of the fission energy defined by ε_D does not pass through the cladding) as follows;

$$q''_L = \frac{q_n f_{assy} f_{rod}}{A_{Heated}} \qquad \text{Eq. 5-107}$$

where

f_{rod} = user-input hot rod peaking factor
q_n = nodal heat rate leaving the cladding in the current node n
A_{Heated} = heated area of the fuel pins in the node

The assembly hot channel factor is selected to represent the local fluid conditions near the hottest pin. The user selects the factor to account for local mixing effects (or lack of mixing). {{

}}$^{2(a),(c)}$

5.7 Material Properties

Material properties are modeled as follows:

Steam Generator Tube Materials: Selected material properties are necessary to model conduction through the SG tubes. Values of the appropriate material for thermal conductivity, specific heat, and steel density are input by the user from standard references. Values are maintained constant for the duration of an analysis.

Fuel Rod Materials: Modeling of conduction within fuel rods is necessary to predict fuel temperature feedback on neutron kinetics calculations. Except for fuel conductivity described below, the material properties for fuel and cladding are taken from standard reference sources such as MATPRO (Reference12.1.33) and maintained constant for the duration of an analysis.

Fuel Conductivity: Temperature-dependent fuel conductivity is calculated during the transient using Eq. (2-52) from Reference 12.1.34 without the gadolinium degradation effect or annealing of irradiation defects terms. The first order burnup effect of the reference equation is also implemented, but higher-order annealing effects are neglected. The conductivity relation from the reference {{

}}$^{2(a),(c)}$

5.8 Numerical Solution

The numerical solution techniques have already been described for the main model parts, namely the thermal hydraulics, the point neutron kinetics, and the pin heat conduction. The overall numerical solution applies the same time step size to these model parts and applies them in sequence. In that way, the {{

}}$^{2(a),(c)}$

{{

}}[2(a),(c)]

After converging to a steady-state solution that is not necessarily stable, the transient calculations are performed as follows:

- The point kinetics model is solved implicitly to update the fission energy term.
- The fraction of the fission energy deposited in the pellets is used in the pin heat conduction model to calculate the heat transfer at the clad surface. This term is added to the direct energy deposition to obtain the energy source term in the coolant. The conduction model is also used to get pellet temperature for Doppler reactivity to be used in the subsequent time step.
- The SG model is integrated to get the heat transfer from the primary coolant loop control volumes in contact with the SG secondary side.
- The core heat source term and the SG heat sink term are used in the thermal-hydraulic explicit solution of the fluid flow conservation equations. Mass flow rate, void fraction, and temperature fields are calculated. The coolant temperature in the core section is used to calculate the moderator temperature reactivity term for using in the subsequent time step point kinetics solution.

The stability of the calculated flow is optionally examined by introducing a user-defined perturbation. This perturbation is typically accomplished by {{

}}[2(a),(c)]

{{

}}2(a), (c)

Figure 5-3. Computational flow chart of the major blocks in the PIM code

6.0 Stability Testing and PIM Code Assessment

The analytical and numerical results make a complete picture of the natural circulation loop stability when relevant experimental data are included. For this purpose, test data from the NIST-1 facility are utilized. Stability tests were conducted in the NIST-1 facility to assess primary system stability performance in an integral test and to provide information to assess the capability of code models to predict the stability behavior. The following subsections describe the facility, test results, and code assessment results.

6.1 Stability Testing in the NuScale Integral System Test Facility

The NIST-1 facility at Oregon State University simulates the thermal-hydraulic operation of the NPM at prototypical primary loop conditions. The facility includes an integrated RPV that houses an electrically-heated core bundle, a helical-coil SG, and a pressurizer.
{{

}}2(a),(c)

6.2 Testing Techniques and Results

Two testing techniques were used to allow the extraction of stability information from the NIST-1 facility. {{

}}[2(a),(c)]

{{

}}[2(a),(c)]

Figure 6-1. Example of NuScale Integral System Test power excitation and the resulting primary flow rate

{{

}}2(a),(c)

Figure 6-2. Example of NuScale Integral System Test steam generator feedwater flow excitation and resulting primary flow rate

{{

}}2(a),(c)

{{

}}2(a),(c)

Figure 6-3. Example of autocorrelation function extracted from a 10-hour NuScale Integral System Test primary flow signal

{{

}}2(a),(c)

Table 6-1. Decay Ratio and Period Results (Test Type I perturbed by power and feedwater flow, and Test Type II is noise analysis with autocorrelation function).

{{

}}2(a),(c)

6.3 Code Assessment Results

Section 5.0 presents the model for stability analysis, including detailed governing equations. The computer code PIM embodies the model presented. Predictions of the PIM code are compared the NIST-1 test data in this section to demonstrate the capability of the code to predict accurate stability results. In performing the assessment, analyses of NIST-1 tests at {{

}}$^{2(a),(c)}$

Figure 6-4. NuScale Integral System Test experimental data and PIM prediction of primary flow response to a feedwater flow excitation at 160 kW

{{

}}$^{2(a),(c)}$

The decay ratio and period are estimated for all the cases by considering the first three or four peaks following the initial perturbation and applying Eq. 6-1. Table 6-2 provides the results for predicted decay ratio and period from PIM for analyzed power levels, with

the corresponding measured values. {{

}}2(a),(c)

Table 6-2. Decay Ratio and Period for Measured and PIM-calculated NuScale Integral System Tests

{{

}}2(a),(c)

The decay ratio and period for all the PIM code runs at different power levels are plotted together with the NIST-1 measured values in Figure 6-5 and Figure 6-6.

{{

}}[2(a),(c)]

Figure 6-5 NuScale Integral System Test-measured and PIM-calculated decay ratios

{{

}}2(a),(c)

Figure 6-6 NuScale Integral System Test-measured and PIM-calculated oscillation period

The predicted decay ratio and period from PIM are in overall acceptable agreement with the data when considering that the highly stable nature of the tests and the predictions make it difficult to interpret results. Overall, predicted decay ratios are {{ }}2(a),(c) than the measured values, which is in the conservative direction for assessing NPM stability.

6.4 Stability Test and Assessment Conclusions

Comparison of the NIST-1 test data with the PIM code predictions shows the PIM code has a conservative bias for the predicted decay ratio of primary system flow peaks that occur immediately after a feedwater flow perturbation. This difference is acceptable because it demonstrates the PIM code provides conservative predictive model for stability analysis of the NPM. Additionally, stability tests performed in the NIST-1 facility demonstrate the stable response of the scaled test facility for primary flow stability. The results of the NIST-1 testing cannot be directly used to draw conclusions about the stability of the NPM, because the NIST-1 facility is not scaled to preserve stability behavior, and different stability parameters and trends are not guaranteed between the two. The important result is that PIM results for the NIST-1 simulation runs agree well with the data, which confirms the suitability of the embedded models. This confirmation provides the needed assurance that these models are accurate for analyzing the NPM stability.

7.0 Support from First Principles Analysis

In this case, first principles analysis is possible only with simplifying assumptions, but it provides valuable insights into the physical nature of the stability problem. It completes the set of tools needed to understand and quantify the stability of the NPM. These tools and mutual links are:

- The PIM code is the main stability analysis tool. Preceding sections presented detailed code models and numerical techniques.
- Stability testing in the NIST-1 facility. The results of these tests, presented in preceding section, cannot be compared directly to the NPM since the NIST-1 facility is not scaled for stability. Instead, the NIST-1 stability results are compared with PIM calculations to validate the code models and thus validated the code can be applied with confidence to NPM.
- First principles analysis. Simplified models are used to provide decay ratio estimates that are free from numerical diffusion problems, which historically caused code results in the BWR context to be suspected of underestimating decay ratios. First principles analysis can be used to study stability trends beyond the range of possible experiments. Additionally, first principles can be used to provide scaling information, which help the basic understanding of test results as they apply the full scale NPM.

The next two subsections present first principles analyses. The first one presents a stability analogue for a single-phase natural circulation loop with the simplifying assumption of an idealized heat sink. The second one presents an analysis of the stability trend if the idealized heat sink assumption were to be relaxed.

7.1 Stability Analogue

A simplified analogue for the flow in the main loop of the NPM is accessible for analytical solution. The loop geometry consists of a fixed-power heater representing a nuclear core that is short compared to the riser section. The loop is closed by the cold leg downcomer where the heat sink heat exchanger is placed at the top of the cold leg. The simple analogue is idealized such that the heat exchanger is so efficient that the temperature (and density) in the cold leg remain constant regardless of the temperature variations of the fluid coming from the riser section. This idealization can be realized by substituting the closed-loop geometry with an open-loop geometry in which the cold leg is substituted by a large tank to impose constant pressure drop boundary condition. The analogue and results are described in References 12.1.16 and 12.1.35. An overview of Reference 12.1.16 is provided here.

The dynamic momentum equation is given as a balance between the buoyancy force generated by the density difference between the riser and the cold leg, and the friction forces along the flow path. Thus,

$$I \frac{d \dot{m}}{dt} = \Delta P_{buoyancy} - \Delta P_{fric} \qquad \text{Eq. 7-1}$$

where

$\dot{m}$	=	mass flow rate
I	=	loop inertia, sum of length-to-area ratio of all sections of the loop
$\Delta P_{buoyancy}$	=	buoyancy drive head
ΔP_{fric}	=	friction pressure drop
t	=	time

The buoyancy term in the steady state is obtained from

$$\Delta P_{buoyancy} = -g\ L\ \Delta\rho = g\ L \rho\ \beta\ \Delta T \qquad \text{Eq. 7-2}$$

where

g	=	gravitational acceleration
L	=	loop height over which the density contrast is present
ρ	=	coolant density
β	=	coolant coefficient of thermal expansion
ΔT	=	temperature difference between the riser and cold leg

The temperature difference between the riser and cold leg is obtained from the energy balance across the heater representing the reactor core. Thus,

$$\Delta T = \frac{Q}{c_p\, \dot{m}} \qquad \text{Eq. 7-3}$$

where

Q	=	heater power
c_p	=	coolant heat capacity

Combining Eq. 7-2 and Eq. 7-3, the steady state buoyancy term is obtained from

$$\Delta P_{buoyancy} = \frac{g\ L\ \rho\ \beta\ Q}{c_p\, \dot{m}} \qquad \text{Eq. 7-4}$$

The friction term is taken as proportional to the square of the mass flow rate. Thus,

$$\Delta P_{fric} = \xi \dot{m}^2 \qquad \text{Eq. 7-5}$$

where the friction coefficient, ξ, is obtained by equating the buoyancy and friction forces at steady state to get

$$\xi = \frac{g\,L\,\rho\,\beta\,Q}{c_p\,\dot{m}_0^3} \qquad \text{Eq. 7-6}$$

where

$\dot{m}_0$ = steady state mass flow rate

The buoyancy head under transient conditions is obtained using the average density along the riser section, given constant cold leg density, thus

$$\Delta P_{buoyancy}(t) = \frac{g\,L\,\rho\,\beta\,Q}{c_p\,\tau_0} \int_0^{\tau_0} \frac{dt'}{\dot{m}(t-t')} \qquad \text{Eq. 7-7}$$

where the integral used for the averaging is taken over the interval, τ_0, which is the time period it takes for a change in density resulting from a change in heating to completely fill the riser.

Combining Eq. 7-1, Eq. 7-5, and Eq. 7-7, the momentum equation for the flow in the natural circulation loop forms the Integro-difference-differential equation,

$$I\,\frac{d\,\dot{m}}{dt} = \frac{g\,L\,\rho\,\beta\,Q}{c_p\,\tau_0} \int_0^{\tau_0} \frac{dt'}{\dot{m}(t-t')} - \xi\dot{m}^2 \qquad \text{Eq. 7-8}$$

The linearized form of Eq. 7-8 is

$$\frac{d\,\delta\dot{m}(t)}{dt} = -\frac{a}{\tau_0} \int_0^{\tau_0} \delta\dot{m}(t-t')\,dt' - 2a\;\delta\dot{m}(t) \qquad \text{Eq. 7-9}$$

where $\delta\dot{m}$ is the flow perturbation, and the coefficient, a, is obtained from

$$a = \frac{g\,L\,\rho\,\beta\,Q}{c_p\,\dot{m}_0^2\,I} \qquad \text{Eq. 7-10}$$

lends itself to analytical and non-diffusive numerical solutions.

Eq. 7-8 or its linearized form Eq. 7-9 represents the riser mode of stability because the cold leg is decoupled by assuming its density is constant. The coefficient given in Eq. 7-10 and the time delay provide for scaling parameters to compare the stability performance of different systems.

7.1.1 Decay Ratio Estimate and Proof of Unconditional Stability of the Riser Mode

Eq. 7-9 is transformed to an algebraic equation by substituting

$$\delta \dot{m}(t) \sim e^{(\sigma + i\omega)t} \qquad \text{Eq. 7-11}$$

where

ω = oscillation frequency
σ = damping coefficient

Separating the real and imaginary parts, we get the following two transcendental equations in σ and ω,

$$1 + 2\tau_0\sigma + \frac{\tau_0}{a}\left(\sigma^2 - \omega^2\right) = e^{-\sigma\tau_0}\cos\omega\tau_0 \qquad \text{Eq. 7-12}$$

$$2\omega\tau_0\left(1 + \frac{\sigma}{a}\right) = -e^{-\sigma\tau_0}\sin\omega\tau_0 \qquad \text{Eq. 7-13}$$

Equations Eq. 7-12 and Eq. 7-13 can be solved numerically for a given pair (a, τ_0) to get (σ, ω). The decay ratio is calculated from

$$DR = \exp\left(2\pi\sigma/\omega\right) \qquad \text{Eq. 7-14}$$

and the oscillation period from

$$T = \frac{2\pi}{\omega} \qquad \text{Eq. 7-15}$$

When the instability threshold condition, $\sigma = 0,$ is imposed on Eq. 7-13, we get

$$\frac{\sin\omega\tau_0}{\omega\tau_0} = -2 \qquad \text{Eq. 7-16}$$

which is an impossible result and a contradiction; therefore; the riser mode is unconditionally stable.

To quantify the decay ratio, numerical solutions were obtained for a wide range of the pair (a, τ_0), which span both the NPM and NIST-1 geometry and operating conditions. The interesting result is that the decay ratio of approximately 0.04 is obtained, signifying a high degree of stability, with minor variation due to the choice of the coefficients (a, τ_0). This rather low decay ratio is approximately the same as the measured NIST-1 decay ratio, and comparable to PIM results for NPM at high power.

Without this result, and since the NIST-1 and the NPM systems generally have different coefficients (a, τ_0), the NIST-1 results could not be applied directly to draw NPM stability conclusions. The NIST-1 results are doubly useful, first to validate the models of PIM,

and second by direct inference with NPM for situations in which the riser dynamics are dominant considering the fixed cold leg density assumption to apply.

An important result from the analogue provided in References 12.1.16 and 12.1.35 is that the system is destabilized when the buoyancy term is sufficiently amplified, which is the case when riser boiling is allowed. This result is reproduced by the PIM code.

Another result from the analogue provided in References 12.1.16 and 12.1.35 is that the negative moderator reactivity feedback is stabilizing. This effect is explained with regard to a positive flow perturbation, which lowers the moderator temperature and increases power due to the reactivity feedback. The increasing power reduces the core exit temperature and dampens the riser density head response. This result is reproduced by the PIM code where a negative MTC is stabilizing, and vice versa.

7.2 Stability Trend with Variation of Power

The results from the stability analogue are limited by the main assumption of frozen cold leg density. An integral relaxation of this assumption in the analogue results in a higher order system in which intuitive insights become difficult to attain. Instead, the cold leg temperature (and density) response to flow perturbation is treated as a separate effect and studied using a simple model for the SG as the heat sink.

Consider a relatively short SG compared with the height of the cold leg, which is consistent with the assumption of short heater relative to the riser height in the original analogue.

{{

}}2(a),(c)

{{

}}2(a),(c)

{{

}}[2(a),(c)]

{{

}}2(a),(c)

Figure 7-1. Decay ratio trend as a function of power for the NuScale Power Module and the NuScale Integral System Test

8.0 Stability Demonstration within Allowable Conditions and Settings

Section 5.0 presented the NuScale model for stability analysis. The computer code PIM, which embodies the model presented, performs analysis for the stability of the NPM at different conditions. The code also performs sensitivity analysis to verify the theoretical trends affecting stability.

The purpose of this section is to analyze the NPM over a wide range of power and primary system flow operating conditions and possible scenarios to demonstrate that stability is maintained. This section focuses on demonstrating stability performance when the plant systems remain within MPS settings (e.g., a reactor trip is not relied on to protect against occurrence of instability). Scenarios in which MPS setpoints are exceeded and a reactor trip occurs are identified in this section and described in Section 9.0.

The operating states and events covered include:

- Stability of various steady-state operating power levels (at the corresponding natural circulation flow) is analyzed to demonstrate the operating behavior with regard to the stability of the NPM during power operations. Stability at BOC and EOC conditions are verified, which addresses moderator reactivity variations in a representative design.

- Stability during transients is analyzed to demonstrate the operating behavior of the NPM during operational events, such as minor changes in feedwater flow, that may occur during normal operations and during AOOs. Also considered is the behavior of the plant to respond to gradual trends in feedwater flow, in which core thermal power responds to changing primary coolant conditions. Specifically, in the calculations presented, the plant is demonstrated to return to stable plant operations, possibly at a new power/flow condition, for any situation in which the riser subcooling is maintained (riser subcooling is protected by the hot leg trip setpoint).

- Stability during heatup at subcritical conditions is analyzed to demonstrate the operating behavior of the NPM during heatup using a non-nuclear heat source. Specifically, the calculations presented show that the plant does not experience unstable flow conditions as the system is brought to conditions necessary for initial criticality. This demonstration includes the effects of the non-nuclear heat source.

8.1 Stability Analysis for a Range of Steady-State Operating Conditions

The scope of this section is to demonstrate the stability performance of the NPM during power operations for a range of power and flow conditions in case of a small perturbation in the plant operations. In each analysis, the natural circulation flow rate is commensurate with power level. Primary system flow, core inlet temperature, secondary inlet flow and temperature, and the secondary steam pressure conditions are specified at each power level. Modeling incorporates the effects of ambient heat losses and heat loss through the non-regenerative heat exchange in the CVCS described in Section 3.6 to ensure consistent thermodynamic modeling of plant operations. {{

}}$^{2(a),(c),ECI}$

The entire range of conditions described in Section 3.6 is considered. However, calculations described in detail in this section are performed at representative thermal power levels of 160, 120, 80, 40, 32, and 1.6 MW. These conditions are equivalent to 100, 75, 50, 25, 20, and 1 percent of rated power, respectively. The power level of 32 MW is considered to address effects related to activation of the turbine and feedwater heater system.

After reaching steady state in each calculation, a small perturbation is applied to the steady conditions {{

}}$^{2(a),(c)}$

After the primary system flow is disturbed, the transient response is calculated and time series signals are recorded in output files for examining the system behavior and evaluating its stability. The stability is deduced from the core inlet flow as function of time, and the signal is selected in a time interval during which the signal clarity is optimal. {{

}}$^{2(a),(c),ECI}$

Brief consideration for the early response and the resulting apparent decay ratio is given in this section. However, the overall effect of any small perturbation that allows the system to return to the initial condition is bounded by the response to operational events described in the next section. The primary emphasis of this section is to demonstrate the stability of the long-term transient response.

Analyses are performed at each condition for a duration that represents approximately ten circuits of coolant in the primary system. The time for coolant to make one circuit corresponds to the primary system coolant mass (not including water in the pressurizer) divided by the flow rate. {{

}}$^{2(a),(c)}$

{{

}}[2(a),(c)]

Table 8-1. Primary System Transit Time

{{

}}[2(a),(c),ECI]

A sample of analysis results is presented below that demonstrates the stability of the NPM.

In applying the perturbation for determining stability performance, it is important to recognize that the magnitude of the resulting initial disturbance is not important as long as the disturbance is small enough to introduce no nonlinear effects or to cause flow regime or heat transfer transitions. What is considered is the relative change of a signal as the disturbance propagates in time.

8.1.1 Stability at Rated Power

{{

}}2(a),(c),ECI

{{

}}2(a),(c),ECI

Figure 8-1. Time trace of primary coolant flow response to a perturbation at rated conditions and beginning-of-cycle reactivity

{{

}}2(a),(c),ECI

Figure 8-2. Time trace of heat addition and heat removal response to perturbation at rated conditions and beginning-of-cycle reactivity

{{

}}2(a),(c),ECI

{{

}}2(a),(c),ECI

Figure 8-3. Time trace of primary coolant flow response to a perturbation at rated conditions and end-of-cycle reactivity

{{

}}2(a),(c),ECI

8.1.2 Stability at 120 MW

{{

}}2(a),(c),ECI

{{

}}2(a),(c),ECI

Figure 8-4. Time trace of primary coolant flow response to a perturbation at 120 MW and beginning-of-cycle reactivity

{{

}}2(a),(c),ECI

8.1.3 Stability at 80 MW

{{

}}2(a),(c),ECI

{{

}}2(a),(c),ECI

Figure 8-5. Time trace of primary coolant flow response to a perturbation at 80 MW and beginning-of-cycle reactivity

{{

}}2(a),(c),ECI

{{

}}2(a),(c),ECI

Figure 8-6. Time trace of primary coolant flow response to a perturbation at 80 MW and beginning-of-cycle reactivity after 250 seconds

{{

}}2(a),(c),ECI

8.1.4 Stability at 40 MW

{{

}}2(a),(c),ECI

{{

}}2(a),(c),ECI

Figure 8-7. Time trace of primary coolant flow response to a perturbation at 40 MW and beginning-of-cycle reactivity after 250 seconds

{{

}}2(a),(c),ECI

{{

}}2(a),(c),ECI

Figure 8-8. Time trace of primary coolant flow response to a sine perturbation with a defined period at 40 MW and beginning-of-cycle reactivity after 250 seconds

{{

}}2(a),(c),ECI

{{

}}2(a),(c),ECI

Figure 8-9. Time trace of primary coolant flow response to a perturbation at 40 MW and end-of-cycle reactivity after 250 seconds

{{

}}2(a),(c),ECI

Figure 8-10. Time trace of heat addition and heat removal response to a perturbation at 40 MW power and end-of-cycle reactivity

8.1.5 Stability at 32 MW

{{

}}2(a),(c),ECI

{{

}}2(a),(c),ECI

Figure 8-11. Time trace of primary coolant flow response to a perturbation at 32 MW and beginning-of-cycle reactivity

{{

}}2(a),(c),ECI

8.1.6 Stability at 1.6 MW

{{

}}2(a),(c),ECI

{{

}}2(a),(c),ECI

Figure 8-12. Time trace of primary coolant flow response to a perturbation at 1.6 MW and beginning-of-cycle reactivity

{{

}}2(a),(c),ECI

{{

}}2(a),(c),ECI

Figure 8-13. Time trace of primary coolant flow response to a sine perturbation with a defined period at 1.6 MW and beginning-of-cycle reactivity after 250 seconds

{{

}}2(a),(c),ECI

{{

}}2(a),(c),ECI

Figure 8-14. Time trace of primary coolant flow response to a perturbation at 1.6 MW and end-of-cycle reactivity

8.1.7 Stability at Rated Power with Feedwater Perturbation

{{

}}2(a),(c),ECI

{{

}}2(a),(c),ECI

Figure 8-15. Time trace of primary coolant flow response to a 60-second feedwater perturbation at rated conditions and beginning-of-cycle reactivity

{{

}}2(a),(c),ECI

Figure 8-16. Time trace of heat addition and heat removal response to a 60-second feedwater perturbation at rated conditions and beginning-of-cycle reactivity

{{

}}2(a),(c),ECI

{{

}}2(a),(c),ECI

Figure 8-17. Time trace of primary coolant flow response to a perturbation at rated conditions and end-of-cycle reactivity

8.1.8 Stability at 40 MW with Feedwater Perturbation

{{

}}2(a),(c),ECI

{{

}}2(a),(c),ECI

Figure 8-18. Time trace of primary coolant flow response to a 60-second feedwater perturbation at 40 MW and beginning-of-cycle reactivity

{{

}}2(a),(c),ECI

Figure 8-19. Time trace of heat addition and heat removal response to a 60-second feedwater perturbation at 40 MW and beginning-of-cycle reactivity

{{

}}2(a),(c),ECI

{{

}}2(a),(c),ECI

Figure 8-21. Time trace of primary coolant flow response to a perturbation at 40 MW and end-of-cycle reactivity

8.2 Stability Analysis for Operational Events

{{

}}2(a),(c),ECI

{{

}}2(a),(c),ECI

- {{

}}2(a),(c),ECI

8.2.1 Increase in Heat Removal by the Secondary System

{{

}}2(a),(c),ECI

8.2.1.1 Rated Power Conditions

{{

}}2(a),(c),ECI

{{

}}2(a),(c),ECI

Figure 8-22. Time trace of primary coolant flow response to an increase in feedwater flow at rated power and beginning-of-cycle reactivity

{{

}}2(a),(c),ECI

Figure 8-23. Time trace of heat addition and heat removal response to an increase in feedwater flow at rated power and beginning-of-cycle reactivity

{{

}}2(a),(c),ECI

Figure 8-24. Time trace of primary coolant flow response to an increase in feedwater flow at rated power and end-of-cycle reactivity

{{

}}2(a),(c),ECI

Figure 8-25. Time trace of heat addition and heat removal response to an increase in feedwater flow at rated power and end-of-cycle reactivity

{{

}}2(a),(c),ECI

{{

}}2(a),(c),ECI

Figure 8-26. Time trace of critical heat flux ratio response to an increase in feedwater flow at rated power and beginning-of-cycle reactivity

{{

}}2(a),(c),ECI

Figure 8-27. Time trace of critical heat flux ratio response to an increase in feedwater flow at rated power and end-of-cycle reactivity

8.2.1.2 Event at 32 MW Conditions

{{

}}2(a),(c),ECI

{{

}}2(a),(c),ECI

Figure 8-28. Time trace of primary coolant flow response to an increase in feedwater flow at 32 MW and beginning-of-cycle reactivity

{{

}}2(a),(c),ECI

Figure 8-29. Time trace of heat addition and heat removal response to an increase in feedwater flow at 32 MW and beginning-of-cycle reactivity

{{

}}2(a),(c),ECI

Figure 8-30. Time trace of primary coolant flow response to an increase in feedwater flow at 32 MW and end-of-cycle reactivity

{{

}}2(a),(c),ECI

Figure 8-31. Time trace of heat addition and heat removal response to an increase in feedwater flow at 32 MW and end-of-cycle reactivity

{{

}}2(a),(c),ECI

8.2.2 Decrease in Heat Removal by the Secondary System

{{

}}2(a),(c),ECI

{{

}}2(a),(c),ECI

8.2.2.1 Rated Power Conditions

{{

}}2(a),(c),ECI

Figure 8-32. Time trace of primary coolant flow response to a 50-percent decrease in feedwater flow at rated power and beginning-of-cycle reactivity

{{

}}2(a),(c),ECI

Figure 8-33. Time trace of heat addition and heat removal response to a 50-percent decrease in feedwater flow at rated power and beginning-of-cycle reactivity

{{

}}2(a),(c),ECI

Figure 8-34. Time trace of primary coolant flow response to a 50-percent decrease in feedwater flow at rated power and end-of-cycle reactivity

{{

}}2(a),(c),ECI

Figure 8-35. Time trace of heat addition and heat removal response to a 50-percent decrease in feedwater flow at rated power and end-of-cycle reactivity

{{

}}2(a),(c),ECI

{{

}}2(a),(c),ECI

Figure 8-36. Time trace of CHF ratio response to a 50-percent decrease in feedwater flow at rated power and beginning-of-cycle reactivity

{{

}}$^{2(a),(c),ECI}$

Figure 8-37. Time trace of CHF ratio response to a 50-percent decrease in feedwater flow at rated power and end-of-cycle reactivity

{{

}}$^{2(a),(c),ECI}$

{{

}}2(a),(c),ECI

Figure 8-38. Time trace of coolant temperature response to a 50-percent decrease in feedwater flow at rated power and beginning-of-cycle reactivity

{{

}}2(a),(c),ECI

Figure 8-39. Time trace of coolant temperature response to a 50-percent decrease in feedwater flow at rated power and end-of-cycle reactivity

{{

}}2(a),(c),ECI

8.2.2.2 Event at 32 MW Conditions with 35 Percent Initial Decay Heat

{{

}}2(a),(c),ECI

{{

}}2(a),(c),ECI

Figure 8-40. Time trace of primary coolant flow response to a 50-percent decrease in feedwater flow at 32 MW and BOC reactivity with 35-percent decay heat

{{

}}2(a),(c),ECI

Figure 8-41. Time trace of heat addition and heat removal response to a 50-percent decrease in feedwater flow at 32 MW and beginning-of-cycle reactivity with 35-percent decay heat

{{

}}2(a),(c),ECI

Figure 8-42. Time trace of primary coolant flow response to a 50-percent decrease in feedwater flow at 32 MW and end-of-cycle reactivity with 35-percent decay heat

{{

}}$^{2(a),(c),ECI}$

Figure 8-43. Time trace of heat addition and heat removal response to a 50-percent decrease in feedwater flow at 32 MW and end-of-cycle reactivity with 35-percent decay heat

{{

}}$^{2(a),(c),ECI}$

8.2.3 Decrease in Reactor Coolant System Flow Rate

{{

}}$^{2(a),(c),ECI}$

8.2.4 Increase in Reactor Coolant Inventory

{{

}}2(a),(c),ECI

8.2.5 Reactivity and Power Distribution Anomalies

{{

}}2(a),(c),ECI

{{

}}2(a),(c),ECI

Figure 8-44. Time trace of primary coolant flow response to an increase in core reactivity at 32 MW and beginning-of-cycle reactivity

{{

}}2(a),(c),ECI

Figure 8-45. Time trace of heat addition and heat removal response to an increase in core reactivity at 32 MW and beginning-of-cycle reactivity

{{

}}2(a),(c),ECI

Figure 8-46. Time trace of primary coolant flow response to an increase in core reactivity at 32 MW and end-of-cycle reactivity

{{

}}2(a),(c),ECI

Figure 8-47. Time trace of heat addition and heat removal response to an increase in core reactivity at 32 MW and end-of-cycle reactivity

{{

}}2(a),(c),ECI

{{

}}2(a),(c),ECI

Figure 8-48. Time trace of critical heat flux ratio response to an increase in core reactivity at 32 MW and beginning-of-cycle reactivity

{{

}}2(a),(c),ECI

Figure 8-49. Time trace of critical heat flux ratio response to an increase in core reactivity at 32 MW and end-of-cycle reactivity

8.2.6 Decrease in Reactor Coolant Inventory

{{

}}2(a),(c),ECI

8.2.7 Effect of Oscillating Feedwater Flow

{{

}}2(a),(c),ECI

Figure 8-50. Time trace of primary coolant flow response to feedwater flow oscillation with a defined period and end-of-cycle conditions

{{

}}2(a),(c),ECI

Figure 8-51. Time trace of heat addition and heat removal response to feedwater flow oscillation with a defined period and end-of-cycle conditions

{{

}}2(a),(c),ECI

8.2.8 Stability During Shutdown by Feedwater Reduction

{{

}}2(a),(c),ECI

{{

}}2(a),(c),ECI

Figure 8-52. Time trace of primary coolant flow response for gradual feedwater reduction at beginning-of-cycle reactivity

{{

}}2(a),(c),ECI

Figure 8-53. Time trace of heat addition and heat removal response for gradual feedwater flow reduction at beginning-of-cycle reactivity

{{

}}2(a),(c),ECI

Figure 8-54. Time trace of primary coolant flow response from 5000 seconds to end of the analysis for a gradual feedwater flow reduction at beginning-of-cycle reactivity

{{

}}2(a),(c),ECI

8.2.9 Stability During Non-Nuclear Heatup (Before Criticality)

{{

}}2(a),(c),ECI

{{

}}2(a),(c),ECI

{{

}}2(a),(c),ECI

Figure 8-55. Time trace of equipment heat rates during the heatup phase

{{

}}2(a),(c),ECI

Figure 8-56. Time trace of system pressurization during the heatup phase

{{

}}2(a),(c),ECI

Figure 8-57. Time trace of coolant and saturation temperatures during the heatup phase

{{

}}2(a),(c),ECI

Figure 8-58. Time trace of primary coolant flow calculated with artificial perturbations during the heatup phase

{{

}}$^{2(a),(c),ECI}$

Figure 8-59. Zoom of core flow showing the time trace of coolant flow damped oscillations in response to an artificial perturbation

{{

}}$^{2(a),(c),ECI}$

9.0 Demonstration of Module Protection System to Preclude Instability

In certain circumstances, the NPM relies on actuation of the MPS to preclude onset of unstable conditions during an operational event. As demonstrated in this section, the MPS actuation occurs in time to prevent the onset of oscillations.

Of the events to be considered, those relying on a trip related to loss of subcooling in the riser are the only events that are important in stability protection. If left unmitigated, the loss of subcooling could lead to undamped flow instabilities.

9.1 Decrease in Heat Removal by the Secondary System

Stability following reduction of feedwater flow for a condition in which the moderator reactivity coefficient is set to zero is explored in this section as a follow-on to Section 8.2.2. In the earlier section, core power responds quickly enough to changes in the loss of heat removal so that saturated conditions in the riser do not occur as shown in Figure 8-38. This section provides analysis results that show the effects of having a zero moderator reactivity coefficient, such that core power only responds to changes in fuel temperature and not to changes in coolant temperature.

Results for the event are provided below. {{

}}2(a),(c),ECI

{{

}}2(a),(c),ECI

Figure 9-1. Time trace of coolant temperature response to a 50-percent decrease in feedwater flow at rated power and zero moderator reactivity feedback

{{

}}2(a),(c),ECI

Figure 9-2. Time trace of primary coolant flow response to a 50-percent decrease in feedwater flow at rated power and zero moderator reactivity feedback

{{

}}2(a),(c),ECI

Figure 9-3. Time trace of heat addition and heat removal response to a 50-percent decrease in feedwater flow at rated power and zero moderator reactivity feedback

{{

}}2(a),(c),ECI

Figure 9-4. Time trace of void fraction response to a 50-percent decrease in feedwater flow at rated power and zero moderator reactivity feedback

{{

}}2(a),(c),ECI

Figure 9-5. Time trace of CHFR response to a 50-percent decrease in feedwater flow at rated power and zero moderator reactivity feedback

9.2 Decrease in Reactor Coolant Inventory

{{

}}2(a),(c),ECI

{{

}}2(a),(c),ECI

{{

}}2(a),(c),ECI

Figure 9-6. Time trace of programmed system pressure at rated power

{{

}}2(a),(c),ECI

Figure 9-7. Time trace of coolant temperature response to a depressurization at rated power and beginning-of-cycle reactivity feedback

{{

}}2(a),(c),ECI

Figure 9-8. Time trace of primary coolant flow response to a depressurization at rated power and beginning-of-cycle reactivity feedback

{{

}}2(a),(c),ECI

Figure 9-9. Time trace of heat addition and heat removal response to a depressurization at rated power and beginning-of-cycle reactivity feedback

{{

}}2(a),(c),ECI

Figure 9-10. Time trace of void fraction response to a depressurization at rated power and beginning-of-cycle reactivity feedback

{{

}}2(a),(c),ECI

Figure 9-11. Time trace of critical heat flux ratio response to a depressurization at rated power and beginning-of-cycle reactivity feedback

{{

}}2(a),(c),ECI

{{

}}2(a),(c),ECI

Figure 9-12. Time trace of primary coolant flow limit-cycle response more than 120 seconds to a depressurization at rated power and beginning-of-cycle reactivity feedback

{{

}}2(a),(c),ECI

{{

}}2(a),(c),ECI

Figure 9-13. Time trace of primary coolant flow response to a depressurization at rated power and end-of-cycle reactivity feedback

{{

}}2(a),(c),ECI

Figure 9-14. Time trace of void fraction response to a depressurization at rated power and end-of-cycle reactivity feedback

{{

}}2(a),(c),ECI

{{

}}2(a),(c),ECI

Figure 9-15. Time trace of primary coolant flow response more than 120 seconds to a depressurization at rated power and end-of-cycle reactivity feedback

10.0 Stability Methodology

The physical basis of the stability analysis methodology was developed and presented in detail in the preceding sections. A phenomena identification and ranking table (PIRT) was created and used as basis for developing the stability analysis code that has been exercised over a wide range of operating conditions and transients. Post-analysis examination of the high-ranking phenomena was presented, and the general characteristics of the stability behavior were established. This physical basis substantiates for the stability analysis methodology.

The purpose of this section is to present two aspects of the stability methodology. The first aspect pertains to the selection of regional exclusion as the solution type and the rationale for this selection.

The second aspect pertains to the type and scope of the generic analysis that supports the definition of the region to be excluded, and the margins and MPS trips that enforce it. These elements constitute the stability analysis application methodology.

10.1 Revisiting High-Ranking Phenomena

{{

}}2(a),(c),ECI

{{

}}2(a),(c),ECI

10.2 General Stability Characteristics

{{

}}2(a),(c),ECI

{{

}}2(a),(c),ECI

Figure 10-1 Illustration of decay ratio band as function of riser subcooling showing range of stability, possible instability, and safety margin

{{

}}2(a),(c),ECI

{{

}}2(a),(c),ECI

10.3 Stability Protection Solution

There are two stability protection types, which emerged from a long history of licensing the operation of BWRs. These types are detect and suppress and regional exclusion. The main features of these two types are presented below with the rationale for adopting the regional exclusion type in this methodology.

- Detect and suppress stability solution. This is an automated solution in which in-core instrumentation signals are processed and oscillation detection algorithms are applied continuously to identify the onset of unstable oscillations. The system is functioning over a wide operational domain defined on a two-dimensional power-flow operating map. Reactor trip set points are based on statistical methods with assumed distributions of oscillation frequency and decay ratios, taking into account reactor trip delays. The system is sufficiently sensitive that it can respond to global and regional mode instabilities and suppress them before thermal limits are violated. The detect and suppress solution is used by most BWR utilities because it can efficiently protect the fuel automatically without reliance on operator action. The advantages for BWRs include the system's ability to detect regional out-of-phase

oscillations that are not manifest in the average neutron flux signals, and doing so on a short time scale that cannot be reliably managed by human operators. These two advantages are not applicable to the NPM: regional mode oscillations are not possible and the oscillation period is significantly longer than in BWRs.

- Regional exclusion stability solution. This solution depends on *a priori* identification of a conservative region on the two-dimensional power-flow map for BWRs in which stability code analysis identifies the possibility of instabilities at any point in the operational cycle. This analysis is validated for each fuel cycle. The identified exclusion region is protected by an automatic reactor trip. A large region is identified which requires manual action to exit the exclusion region to avoid unnecessary trips. This solution is less favored by BWR utilities because the exclusion region is often too large and conservatively defined which reduces operational flexibility.

In the case of the NPM, regional exclusion solution is the appropriate stability solution. The rationale for this selection is presented.

- Automatic oscillation detection is not needed because the incipience and growth of the oscillation in the NPM is slow, where the characteristic period is an order of magnitude or longer compared with BWR oscillations. With such a slow transient, normal operation maneuvers could be confused for instabilities.

- The exclusion region for an NPM is not a two-dimensional area on a power-flow map that requires extensive cycle-specific analysis to define; rather, the exclusion region is one-dimensional defined as a point on the riser subcooling (or temperature as a function of pressure) range.

- The riser subcooling is protected by automatic action for other purposes. Therefore, stability protection requires no new analysis or equipment.

- The analysis that supports the claim that instabilities in the NPM are possible only when riser voiding occurs is not needed on a cycle-specific basis. The analytical methodology to support this claim using the stability PIM code is extensive because it is a unique analysis.

In conclusion, the selected stability protection solution for the NPM is the regional exclusion solution. The region is defined by a single point specifying riser subcooling margin. The stability exclusion region is protected by automatic action. Section 10.4 describes stability analysis application methodology using the PIM code.

10.4 Stability Analysis Application Methodology

The stability application methodology is defined by the transient PIM code and the range of conditions to be analyzed to support the claim that the NPM is stable, given that riser subcooling is maintained.

The application methodology described in this section addresses key considerations in applying the computational methods of this topical report for calculations related to

confirming the NPM stability performance. The application methodology addresses evolving design, performance, and operation by analyzing the effect of such evolutions in the stability analysis. Changes may stem from effects such as revision of the plant design, improved hydraulic and neutronic design of the nuclear fuel, cycle length changes, power uprates, and cycle-specific application (e.g., the initial core).

The following considerations are made in confirming the NPM stability performance and acceptability of the regional exclusion solution when addressing evolving design, performance, or operation of the NPM. These considerations are the key parameters affecting NPM stability performance. {{

}}[2(a),(c)]

Demonstration examples of the scope of analysis conditions are provided in this report to support the applicability of the analytical methods of the PIM code. Final analysis will be provided separately for the final design. An application of this methodology with a full analysis scope is expected to support or disposition the stability impact of future NPM design changes.

In order to utilize the methodology described in this report, the applicability of the regional exclusion stability protection solution by satisfying the condition that the conservative maximum (positive) MTC is within the value used for the generic analysis and the riser subcooling is within the technical specification value must be confirmed on a cycle-specific basis.

11.0 Summary and Conclusions

A methodology for the evaluation of the stability of the NPM has been presented. The stability phenomena are considered from the fundamental level and screened for applicability to NPM. The ranking of these phenomena is the guide for the computational models developed for the stability analysis and is assessed versus NIST-1 data and supported by first principles analysis of trends.

No assumptions are made with regard to stability trends being in any way similar to past experience, particularly with BWRs. Important differences between BWR and the NPM stability trends are identified, namely: {{

}}2(a),(c),ECI

The NPM primary coolant flow is found to be stable for the entire operational domain for the analyzed conditions. This finding is based on a wide range of exploratory calculations with varied operating conditions and assumptions. Uncertainty analysis does not identify the possibility of destabilization compared with the best-estimate hydraulic characterization.

Instabilities can be excited only when operating outside the design range in which riser voiding becomes possible. These instabilities are prevented by the reactor protection system being triggered by trip setpoints on reactor pressure or core exit subcooling violations. Simulating transients with growing oscillations destabilized by riser voiding do not challenge SAFDLs in the example cases. For EOC, the negative moderator coefficient suppresses the oscillation growth; while for BOC, the oscillations reach a large amplitude limit cycles without significant loss of CHF margin. However, as benign as these oscillations may be, the stability analysis methodology conservatively prevents their occurrence.

The proposed stability protection solution for the NPM belongs in the class of regional exclusion. The analytical methods support the identification of the unstable operating region as the one in which riser voiding is possible regardless of the cause of the loss of

riser subcooling margin (e.g., high power, low pressure, or degraded SG heat sink). The MPS trip enforces the exclusion region. The licensing basis of the identification of the exclusion region is generic and applicable to the final design, and confirmation analysis is necessary in the case of design updates as explained in Section 10.0 above.

12.0 References

12.1 Referenced Documents

12.1.1 NuScale Power, LLC, "NuScale Topical Report: Quality Assurance Program Description for the NuScale Power Plant," NP-TR-1010-859-NP, Rev. 3, January 2016.

12.1.2 U.S. Nuclear Regulatory Commission, Design-Specific Review Standard for NuScale SMR Design, “Thermal Hydraulic Stability Review Responsibilities” Section 15.9.A, Rev. 0, June 2016 (ML15355A311).

12.1.3 R. T. Lahey, Jr. and D. A. Drew, "An Assessment of the Literature Related to LWR Instability Modes," NUREG/CR-1414, April 1980.

12.1.4 J. A. Bouré, A. E. Bergles, and L. S. Tong, "Review of Two-Phase Flow Instability," Nuc. Eng. and Design 25 (1973) pp. 165-192.

12.1.5 Carsten Lange, Dieter Hennig, Manuel Schultze, and Antonio Hurtada, "Complex BWR Dynamics from the Bifurcation Theory Point of View," Annals of Nuclear Energy 67 (2014) 91-108.

12.1.6 J. March-Leuba, "Density-Wave Instabilities in Boiling Water Reactors," NUREG/CR-6003, September 1992.

12.1.7 J. March-Leuba and J. M. Rey, "Coupled thermohydraulic-neutronic instabilities in boiling water nuclear reactors: a review of the state of the art," Nuclear Engineering and Design, Volume 145, Issues 1–2, 2 November 1993, Pages 97–111

12.1.8 Design Control Document for the US-APWR, MUAP-DC004, Rev. 3 March 2011, Mitsubishi Heavy Industries.

12.1.9 L. S. Tong and J. Weisman, "Thermal Analysis of Pressurized Water Reactors," American Nuclear Society, Second Edition, 1979.

12.1.10 "Natural Circulation in Water Cooled Nuclear Power Plants – Phenomena, models, and methodology for system reliability assessments," IAEA-TECDOC-1474, November 2005, ISBN 92–0–110605–X

12.1.11 Gonella V. Durga Prasad et al., "Review of Research on Flow Instabilities in Natural Circulation Boiling Systems," Progress in Nuclear Energy 49 (2007) 429-451.

12.1.12 Y. M. Farawila and D. W. Pruitt, "A Study of Nonlinear Oscillation and Limit Cycles in Boiling Water Reactors—II: The Regional Mode," NUCLEAR SCIENCE AND ENGINEERING: 154, 316–327 (2006).

12.1.13 W. Ambrosini, F. D´Auria, A. Pennati, and J. C. Ferreri, "Numerical Effects in the Prediction of Single-phase Natural Circulation Stability," UIT 2001 Conference, Modena, Italy, June 25-27 2001.

12.1.14 J. C. Ferreri and W. Ambrosini, "Verification of RELAP5/MOD3 with Theoretical and Numerical Stability Results on Single-Phase, Natural Circulation in a Simple Loop," NUREG/IA-0151, Feb. 1999.

12.1.15 S. Chandrasekhar, "Hydrodynamic and Hydromagnetic Stability," Dover Publications, Library of Congress number 80-69678.

12.1.16 Y. M. Farawila, D. R. Todd, and M. J. Ades, J. N. Reyes, Jr., “Analytical Stability Analogue for a Single-Phase Natural Circulation Loop,” Accepted for publication in Nuclear Sci. & Engineering, (Submitted Jan. 2016 and accepted June 2016).

12.1.17 UK-EPR Fundamental Safety Overview, Volume 2: Design and Safety, Chapter D: Reactor and Core, Sub-Chapter D.4 Core Thermal-Hydraulic Design, AREVA Inc., undated.

12.1.18 P. Saha, M. Ishii, and N. Zuber, “Experimental investigation of the thermally induced flow oscillations in two-phase systems,” Journal of Heat Transfer, 98(4): 616–622, 1976.

12.1.19 W. Wulff et al., "A Description and Assessment of RAMONA-3B MOD.0 Cycle 4: A Computer Code with Three-Dimensional Neutron Kinetics for BWR System Transients," NUREG/CR-3664, Brookhaven National Laboratory, January 1984.

12.1.20 U. S. Rohatgi et al., "RAMONA-4B – A Computer Code with Three-Dimensional Neutron Kinetics for BWR and SBWR System Transient," NUREG/CR-6359, Vol. 1, Brookhaven National Laboratory, March 1998.

12.1.21 N. Hoyer, "MONA, A 7-Equation Transient Two-Phase Flow Model for LWR Dynamics," Proc. Int. Conf. on New Trends in Nuclear System Thermohydraulics, Pisa, June 1994, Vol. 1, pp. 271 -280.

12.1.22 R. T. Lahey, Jr. and F. J. Moody, "The Thermal-hydraulics of a Boiling Water Reactor," American Nuclear Society, Second Edition, 1993.

12.1.23 "Natural circulation in water cooled nuclear power plants – Phenomena, models, and methodology for system reliability assessments," International Atomic Energy Agency, IAEA-TECDOC-1474, November 2005, ISBN 92–0–110605–X.

12.1.24 Frank P. Incropera, David P. DeWitt, Fundamentals of Heat and Mass Transfer, Third Edition, Wiley and Sons, New York, 1990.

12.1.25 N. E. Todreas and M. S. Kazimi, Nuclear Systems: Vol. I, Thermal Hydraulic Fundamentals, Hemisphere, NY 1990

12.1.26 Release on the IAPWS Formulation 1995 for the Thermodynamic Properties of Ordinary Water Substance for General and Scientific Use, The International Association for the Properties of Water and Steam, Frederica, Denmark, Sept. 1996.

12.1.27 H. Muller-Steinhagen and K. Heck. A simple friction pressure drop correlation for two-phase flow in pipes. Chemical Engineering and Processing, 20(6):297–308, November 1986.

12.1.28 C.F. Colebrook, "Turbulent flow in pipes, with particular reference to the transition region between smooth and rough pipe laws." Journal of the Institution of Civil Engineers, London, February 1939.

12.1.29 The RELAP5-3D Development Team, “RELAP5-3D Code Manual, Volume I: Code Structure, System Models, and Solution Methods,” INEEL-EXT-98-00834-V1, Revision 2.4, Idaho National Laboratory, June 2005

12.1.30 J.G. Collier, Convective Boiling and Condensation, McGraw Hill, London, 1972.

12.1.31 James J. Duderstadt and Louis J. Hamilton, Nuclear Reactor Analysis, 1976.

12.1.32 NP-2609-V2, “Parametric Study of CHF Data, Volume 2: A Generalized Subchannel CHF Correlation for PWR and BWR Fuel Assemblies” Electric Power Research Institute, January 1983.

12.1.33 NUREG/CR-6150, Vol. 4, Rev. 2, “MATPRO -A Library of Materials Properties for Light-Water-Reactor Accident Analysis,”(NRC ADAMS: Part #1, ML010330363 Part #2, ML010330400)

12.1.34 NUREG-CR-7022-V1, “FRAPCON-3.4: A Computer Code for the Calculation of Steady-State, Thermal-Mechanical Behavior of Oxide Fuel Rods for High Burnup” (NRC ADAMS: ML14295A539).

12.1.35 Y. M. Farawila, D. R. Todd, and M. J. Ades, “Analytical Stability Analogue for a Single-Phase Natural Circulation Loop,” 16th International Topical Meeting on Nuclear Reactor Thermal Hydraulics NURETH-16, Chicago, Il, Aug. 30-Sept. 4, 2015.

Appendix A. Stability of the Flow in the Steam Generator Tubes

A.1 Background

The SG is made up of many tubes helically wound to fit within the annulus space of the reactor pressure vessel. The top and bottom of each tube is connected to an upper (steam) plenum and lower (feedwater) plenum, respectively. The individual tubes of the SG are subjected to the same pressure drop between the two plena.

In the SG, heat is transferred from primary-side single-phase fluid passing over the outside of the tubes to the secondary-side fluid within the individual tubes. The primary-side fluid enters the SG at the upper plenum at a temperature that exceeds the saturation temperature of the secondary side. The secondary-side flow enters each individual tube via the lower plenum in a subcooled state. The flow entering each tube is heated by the primary side and is brought to boiling as it travels upward. Heating continues with full conversion of the secondary-side fluid to steam, followed by heat transfer to single-phase steam. The exit condition of the secondary-side fluid from the tube at the upper plenum is superheated steam. The flow in individual tubes of the SG is subject to density wave instabilities depending on the fluid two-phase conditions (e.g., the total power transferred from the primary side), pressure, and inlet subcooling. Therefore, design considerations are made within the NPM SG to prevent instabilities within individual tubes by increasing flow resistance at the lower plenum. However, as part of a comprehensive effort to address the overall stability performance of the NPM within the scope of GDC 10 and GDC 12, it is necessary to understand the effects of instabilities within the SG on the primary side, and particularly for the SAFDLs. Therefore, a parametric evaluation of the effects of flow oscillation on the primary side is provided.

Considering the experience and the considerable literature on density waves in boiling systems, the flow is known to become less stable for higher power, higher inlet subcooling, and lower pressure (References A.1 and A.2). With regard to the axial power distribution, bottom peaking is known to be destabilizing. In the case of the heated tube, a considerable segment of the flow is in two-phase conditions and remains at a constant temperature, while the primary coolant temperature monotonically decreases as it travels downward. Therefore, the temperature difference driving heat transfer is smaller in the bottom of the tube, resulting in shifting the axial heating distribution upwards, which tends to have a stabilizing effect.

The one unique feature of the helical-coil SG tubes that differs from the bulk of the published studies of density wave instabilities is that the SG tubes are not vertical. However, the helical tubes can be considered as inclined tubes assuming the impact of the centrifugal forces on the flow stability to be negligible, and thus the gravitational component of the pressure drop is scaled accordingly in the stability analysis. Therefore, only quantitative, not qualitative, differences are expected compared with the existing analysis and understanding of density waves in boiling channels.

A.2 Density Waves in Parallel Channels

The oscillation mode, in which the flow in the parallel channels oscillates in phase, is not the dominant mode because the net flow entering and leaving the SG also oscillates against the damping forces of the feedwater pumps and friction in the inlet and outlet piping connected to the SG. The damping forces of the components external to the SG are eliminated for the oscillation modes in which phase differences in individual tubes result in cancelling out any oscillations in the total SG flow and the pressure difference between the plena remains constant. In the idealized case in which there are only two tubes, the flow oscillations in one tube are out of phase with the other tube (180 degrees). In the case of three tubes, the preferred phase difference is 120 degrees to maintain constant pressure drop between the plena (See Reference A.3). For four tubes, two preferred mode possibilities exist: either the tubes oscillate with a phase difference of 90 degrees apart from one to the next, or two groups of two tubes each oscillate out of phase while the tubes in each group oscillate in phase with one another. Physically, there is no mechanism that forces the grouping of tubes and locks the channels in each group to oscillate in phase. This phenomenon is unlike the case of BWR fuel bundles in which the flow in half the bundles is locked in phase and oscillates out of phase with the group of bundles in the other half of the core. In the BWR case, the locking mechanism is the excitation of the first azimuthal mode of the neutron flux. A similar mechanism is not present in the helical coil SG design to lock the phase of oscillations in the SG tubes. With hundreds of tubes in the SG, the oscillation phase difference in different tubes can be randomized to create the preferred constant pressure drop between the plena.

A.3 Coupling Between the Primary and Secondary Fluids

The NPM is designed to operate without pumps in the primary system. Flow in the primary side is driven by the density difference between the fluid in the riser, which is heated by the core, and the fluid in the downcomer, which is cooled by the SG.

A perturbation in the flow of the SG tubes creates a corresponding perturbation in the heat transfer from the primary side and downcomer density response, resulting in a reactor coolant flow response. The reactor coolant flow response affects the heat transfer to the SG. This feedback loop coupling does not result in self-sustained instability because the flow response within the SG would be in phase in the tubes and encounters the damping that results from the feedwater pump and piping external to the SG.

In the case of density wave oscillations in the SG tubes, the phase of the oscillation in each of the tubes results in cancelling out any net oscillation effect on the heat transfer and thus no feedback to the reactor coolant loop. It is therefore concluded that there is no possibility of instability due to the coupling between the reactor coolant flow and the flow in the SG tubes.

A.4 Calculations and Results

As described above, the in-phase oscillation of secondary flow does not occur and the out-of-phase oscillatory flow in individual tubes cancel out, so that the net secondary flow is not oscillating. Therefore, the rate of heat transfer from the reactor coolant flow is maintained without oscillation. However, the overall average heat transfer to the SG may be affected. This effect is discussed below.

The overall heat transfer coefficient between the flow inside and outside a tube, h, is obtained from the heat transfer coefficient from the inner surface of the tube to the inside flow, h_{in}, and the outside heat transfer coefficient, h_{out}, accounting for the tube wall and the outer fluid. Thus,

$$h = \frac{1}{\frac{1}{h_{out}} + \frac{1}{h_{in}}} \qquad \text{Eq. A-1}$$

The inner heat transfer coefficient has an oscillating component, assumed sinusoidal, due to flow oscillations inside the tube; thus, the time-dependent overall heat transfer coefficient is obtained from

$$h(t) = \frac{1}{\frac{1}{h_{out}} + \frac{1}{h_{in} + a\sin\omega \mathrm{t}}} \qquad \text{Eq. A-2}$$

where $a < h_{in}$ is the oscillation magnitude, and ω is the oscillation frequency. The average heat transfer coefficient for a number of tubes, N, oscillating at equal phase intervals, is obtained from

$$\overline{h}(t) = \frac{1}{N}\sum_{n=1}^{N} \frac{1}{\frac{1}{h_{out}} + \frac{1}{h_{in} + a\sin\left(\omega \mathrm{t} + 2\pi(n-1)/N\right)}} \qquad \text{Eq. A-3}$$

Notice that for a finite number of tubes, the average heat transfer coefficient is still time dependent where the magnitude of its oscillation is reduced and is retained as a second order effect. Illustrating for the specific case of $N = 2,$ we get

$$\overline{h}_{N=2}(t) = \frac{1}{2}\frac{1}{\frac{1}{h_{out}} + \frac{1}{h_{in} + a\sin\omega \mathrm{t}}} + \frac{1}{2}\frac{1}{\frac{1}{h_{out}} + \frac{1}{h_{in} - a\sin\omega \mathrm{t}}} = \frac{h_{out}h_{in}\left(h_{out} + h_{in}\right) - h_{out}a^2\sin^2\omega t}{\left(h_{out} + h_{in}\right)^2 - a^2\sin^2\omega t} \qquad \text{Eq. A-4}$$

where it can be observed that the average two-tube heat transfer coefficient oscillates with the double frequency of the oscillation in each tube, and oscillates between the steady operation as an upper value and a minimum value when $\sin^2\omega t = 1$. Therefore,

the average heat transfer coefficient over the oscillation period is somewhat diminished. This effect can be explored further for the realistic case of a large number of tubes.

For a large number of tubes, the average heat transfer coefficient becomes independent of time and is obtained from

$$\overline{h} = \frac{1}{2\pi}\int_0^{2\pi} \frac{d\theta}{\dfrac{1}{h_{out}} + \dfrac{1}{h_{in} + a\sin\theta}} = h_{out} - \frac{h_{out}^2}{\sqrt{\left(h_{out} + h_{in}\right)^2 - a^2}} \qquad \text{Eq. A-5}$$

The ratio of the average heat transfer coefficient of many tubes relative to the steady (non-oscillating) value, R, becomes

$$R = \left(1 + \frac{h_{out}}{h_{in}}\right)\left(1 - \frac{h_{out}}{\sqrt{\left(h_{out} + h_{in}\right)^2 - a^2}}\right) \le 1 \qquad \text{Eq. A-6}$$

Physically, the maximum reduction of the inner heat transfer coefficient does not cause it to vanish completely. However, considering this extreme case by using $a = h_{in}$, the minimum relative heat transfer coefficient becomes

$$R_{\min} = \left(1 + \frac{h_{out}}{h_{in}}\right)\left(1 - \frac{h_{out}}{\sqrt{\left(h_{out} + h_{in}\right)^2 - h_{in}^2}}\right) < 1 \qquad \text{Eq. A-7}$$

The minimum relative heat transfer coefficient under the maximum possible inner heat transfer coefficient oscillation magnitude depends on the ratio of the steady flow outer-to-inner heat transfer coefficient. The minimum ratio of $R_{\min} = 0.828$ is attained when the steady flow outer-to-inner heat transfer coefficient ratio, h_{out}/h_{in}, is 0.414.

Even under the extreme assumptions of inner heat transfer coefficient oscillation magnitude and most sensitive heat transfer resistance combination inside and outside the tube, the overall heat transfer coefficient remains steady (not oscillating) with a downshift of only 17 percent. For a realistic design, the heat transfer coefficient drop under severe flow oscillations inside the tubes is only a few percent. For example, an inner heat transfer coefficient oscillation magnitude of 50 percent results in the reduction of the effective heat transfer coefficient by only 3.3 percent under the most sensitive heat transfer corresponding to $h_{out}/h_{in} = 0.9$.

The effect of the overall SG heat transfer coefficient drop due to parallel channel flow oscillations inside the tubes is a gradual increase in the reactor coolant flow temperature, which results in reducing the reactor power due to negative reactivity coefficient until the heat balance is restored at lower power. It is possible that the new steady state under the reduced reactor power would also restore the stability of the flow in the SG tubes. Conversely, reactor reactivity control action to restore the original power

level would result in a slightly higher primary coolant temperature compared with the stable SG flow case. In all conditions, the primary loop flow is driven to oscillate in response to SG instability.

A.5 Conclusions

Based on the information provided in this appendix, it is concluded that the main effect of density waves in the tubes of the helical coil SG is a small reduction in the effective heat transfer coefficient between the two sides of the SG. Unstable flow oscillations impact on heat transfer in individual tubes do not affect the overall heat transfer to the primary side because the flow oscillations in the tubes are not in-phase and thus their individual effects cancel out. Significant primary flow oscillations are not excited by the instabilities in the SG tubes.

A.6 References

A.1 Vladimir B. Khabensky, Vladimir Antonovich Gerliga, Coolant Flow Instabilities in Power Equipment, CRC Press, 2013.

A.2 J. A. Bouré et al., "Review of Two-Phase Flow Instability," Nuc. Eng. & Design 25 (1973) pp. 165-192.

A.3 J. March-Leuba, "Density-Wave Instabilities in Boiling Water Reactors," NUREG/CR-6003, Sept. 1992.

Enclosure 3:

Affidavit, AF-0716-50372

NuScale Power, LLC
1100 NE Circle Blvd., Suite 200 Corvallis, Oregon 97330 Office 541.360-0500 Fax 541.207.3928
www.nuscalepower.com

NuScale Power, LLC

AFFIDAVIT of Thomas A. Bergman

I, Thomas A. Bergman , state as follows:

(1) I am the Vice President of Regulatory Affairs of NuScale Power, LLC (NuScale), and as such, I have been specifically delegated the function of reviewing the information described in this Affidavit that NuScale seeks to have withheld from public disclosure, and am authorized to apply for its withholding on behalf of NuScale

(2) I am knowledgeable of the criteria and procedures used by NuScale in designating information as a trade secret, privileged, or as confidential commercial or financial information. This request to withhold information from public disclosure is driven by one or more of the following:

(a) The information requested to be withheld reveals distinguishing aspects of a process (or component, structure, tool, method, etc.) whose use by NuScale competitors, without a license from NuScale, would constitute a competitive economic disadvantage to NuScale.

(b) The information requested to be withheld consists of supporting data, including test data, relative to a process (or component, structure, tool, method, etc.), and the application of the data secures a competitive economic advantage, as described more fully in paragraph 3 of this Affidavit.

(c) Use by a competitor of the information requested to be withheld would reduce the competitor's expenditure of resources, or improve its competitive position, in the design, manufacture, shipment, installation, assurance of quality, or licensing of a similar product.

(d) The information requested to be withheld reveals cost or price information, production capabilities, budget levels, or commercial strategies of NuScale.

(e) The information requested to be withheld consists of patentable ideas.

(3) Public disclosure of the information sought to be withheld is likely to cause substantial harm to NuScale's competitive position and foreclose or reduce the availability of profit-making opportunities. The accompanying report reveals distinguishing aspects about the method by which NuScale develops its evaluation methodology for stability analysis of the NuScale Power Module.

NuScale has performed significant research and evaluation to develop a basis for this methodology and has invested significant resources, including the expenditure of a considerable sum of money.

The precise financial value of the information is difficult to quantify, but it is a key element of the design basis for a NuScale plant and, therefore, has substantial value to NuScale.

If the information were disclosed to the public, NuScale's competitors would have access to the information without purchasing the right to use it or having been required to undertake a similar expenditure of resources. Such disclosure would constitute a misappropriation of NuScale's intellectual property, and would deprive NuScale of the opportunity to exercise its competitive advantage to seek an adequate return on its investment.

(4) The information sought to be withheld is in the enclosed report entitled "Evaluation Methodology for Stability Analysis of the NuScale Power Module."The enclosure contains the designation "Proprietary" at the top of each page containing proprietary information. The information considered by NuScale to be proprietary is identified within double braces, "{{ }}" in the document.

(5) The basis for proposing that the information be withheld is that NuScale treats the information as a trade secret, privileged, or as confidential commercial or financial information. NuScale relies upon the exemption from disclosure set forth in the Freedom of Information Act ("FOIA"), 5 USC § 552(b)(4), as well as exemptions applicable to the NRC under 10 CFR §§ 2.390(a)(4) and 9.17(a)(4).

(6) Pursuant to the provisions set forth in 10 CFR § 2.390(b)(4), the following is provided for consideration by the Commission in determining whether the information sought to be withheld from public disclosure should be withheld:

(a) The information sought to be withheld is owned and has been held in confidence by NuScale.

(b) The information is of a sort customarily held in confidence by NuScale and, to the best of my knowledge and belief, consistently has been held in confidence by NuScale. The procedure for approval of external release of such information typically requires review by the staff manager, project manager, chief technology officer or other equivalent authority, or the manager of the cognizant marketing function (or his delegate), for technical content, competitive effect, and determination of the accuracy of the proprietary designation. Disclosures outside NuScale are limited to regulatory bodies, customers and potential customers and their agents, suppliers, licensees, and others with a legitimate need for the information, and then only in accordance with appropriate regulatory provisions or contractual agreements to maintain confidentiality.

(c) The information is being transmitted to and received by the NRC in confidence.

(d) No public disclosure of the information has been made, and it is not available in public sources. All disclosures to third parties, including any required transmittals to NRC, have been made, or must be made, pursuant to regulatory provisions or contractual agreements that provide for maintenance of the information in confidence.

(e) Public disclosure of the information is likely to cause substantial harm to the competitive position of NuScale, taking into account the value of the information to NuScale, the amount of effort and money expended by NuScale in developing the information, and the difficulty others would have in acquiring or duplicating the information. The information sought to be withheld is part of NuScale's technology that provides NuScale with a competitive advantage over other firms in the industry. NuScale has invested significant human and financial capital in developing this technology and NuScale believes it would difficult for others to duplicate the technology without access to the information sought to be withheld.

I declare under penalty of perjury that the foregoing is true and correct. Executed on July 31, 2016.

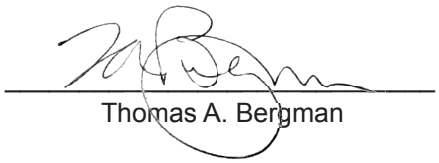

Thomas A. Bergman